Ore Geology Reviews 105 (2019) 258–272

Contents lists available at ScienceDirect

Ore Geology Reviews

journal homepage: www.elsevier.com/locate/oregeorev

Origin of the Mo-bearing Xiaoshuijing Syenogranite in the Tengchong Terrane, SW China

Hao Zou[a,b], Hua-Wen Cao[c,*], Leon Bagas[b,d], Yun-Hui Zhang[e], Shou-Ting Zhang[f], Qiang Zhang[g], Hang Liu[a], Yang Li[a]

[a] State Key Laboratory of Tectonic Controls on Mineralization and Hydrocarbon Accumulation of Ministry of Land and Resources, Chengdu University of Technology, Chengdu, Sichuan 610059, China
[b] Centre of Exploration Targeting, The University of Western Australia, 35 Stirling Highway, Crawley, WA 6009, Australia
[c] Chengdu Centre, China Geological Survey, Chengdu, Sichuan 610081, China
[d] MLR Key Laboratory of Metallogeny and Mineral Assessment, Institute of Mineral Resources, CAGS, Beijing 100037, China
[e] State Key Laboratory of Geohazard Prevention and Geoenvironment Protection, Chengdu University of Technology, Chengdu, Sichuan 610059, China
[f] School of Earth Sciences and Resources, China University of Geosciences, Beijing 100083, China
[g] Faculty of Earth Resources, China University of Geosciences, Wuhan 470074, China

ARTICLE INFO

Keywords:
Xiaoshuijing Syenogranite
Mo mineralisation
LA-ICP-MS, U-Pb zircon age
Re-Os age
Hf isotope
Tengchong Terrane

ABSTRACT

The Xiaoshuijing Syenogranite is the host of Mo mineralisation recently discovered in the Tengchong Terrane of southwestern China. Here, we present new zircon U-Pb ages and molybdenite Re-Os ages, whole-rock geochemical data, and zircon Hf isotopic data for the Xiaoshuijing Syenogranite hosting disseminated Mo mineralisation. The syenogranite's mineralogical and geochemical characteristics indicate it is a high-K, alkaline, and peraluminous granite. LA-ICP-MS analysis of zircon yields an age of 65 ± 1 Ma (n = 14, MSWD = 2.1), and yields negative zircon $\varepsilon_{Hf}(t)$ values ranging from −18.23 to −12.92, interpreted to have a crustal source. The Re-Os Mo age of 64 ± 2 Ma (n = 4, MSWD = 2.2) for the mineralisation is the same as the syenogranite's age, within error. The geochemistry also indicates that the syenogranite is related to a thickened crust resulting from the eastward subduction of the Neo-Tethyan oceanic lithosphere shortly before the collision of the Indian and Eurasian continental crusts.

1. Introduction

The Tethyan Ocean included a series of long-lived oceans separating the Eurasian Plate to the north and the Indian Plate to the south. The oceans opened during the breakup of Gondwanaland and their closure involved collisional tectonics during the formation of the Tethys Tectonic Domain (Fig. 1a). The Sanjiang-Tethys Terrane records a complex tectono-magmatic evolution and contains huge Sn-Cu-Pb-Zn-Ag-Mo-W-Au resources, which have been extensively studied (Pan et al., 2004; Chen et al., 2005, 2006; Deng et al., 2014a,b; Liu et al., 2009; Wang et al., 2014a; Ma et al., 2014; Cao et al., 2016, 2017a, 2017b; Li et al., 2017a; Li et al., 2017b; Zhang et al., 2017; Zhao et al., 2016, 2017; Zhu et al., 2017a,b). The authors of these studies suggest that the Mesozoic to Cenozoic was a period characterised by increased igneous and mineralising events, which are closely related to the subduction of the Meso-Tethyan and Neo-Tethyan oceanic plates.

The Tengchong Terrane is an important part of the Sanjiang-Tethys Terrane in the southwestern China. The terrane has widespread Cretaceous to Cenozoic granites included in the Donghe, Guyong, and Binlang River granitic suites (NRGST, 1985; Chen, 1987; Shi et al., 1989; Liu et al., 1993; Lu et al., 1993 Zhang, 1996; Xia, 2003; Dong et al., 2006; Tao et al., 2009; Yang et al., 2009; Jiang et al., 2012, Xu et al., 2012; Pirajno, 2013; Chen et al., 2015, 1991; Qi et al., 2015). The suites young from NE to SW oblique to the regional foliation (Fig. 1b). The area includes granitic rocks related to with a combination of Sn, Cu, Pb, Zn, Ag and W polymetallic deposits (Wang et al., 2014b; Tao et al., 2010). The recent discovery of Sn mineralisation at the large Xiaolonghe and Lailishan Sn deposits and various small- to medium-size polymetallic occurrences has confirmed the high prospectivity of the region. Examples include the Jiaojiguan (Fe-Cu-Pb-Zn), Tieyaoshan (Sn), Maliba (Pb-Zn-Mo), Baihua'nao (Sn-REE), Xinqi (Sn-W), and Dadongchang (Cu-Pb-Zn) deposits (Chen, 1987; Dong et al., 2005; Hou et al., 2007; Tao et al., 2010; Zhu et al., 2011; Xu et al., 2012; Ma et al., 2013; Wang et al., 2014b).

* Corresponding author.
E-mail address: caohuawen1988@126.com (H.-W. Cao).

https://doi.org/10.1016/j.oregeorev.2018.12.018
Received 15 March 2018; Received in revised form 21 November 2018; Accepted 19 December 2018
Available online 20 December 2018
0169-1368/

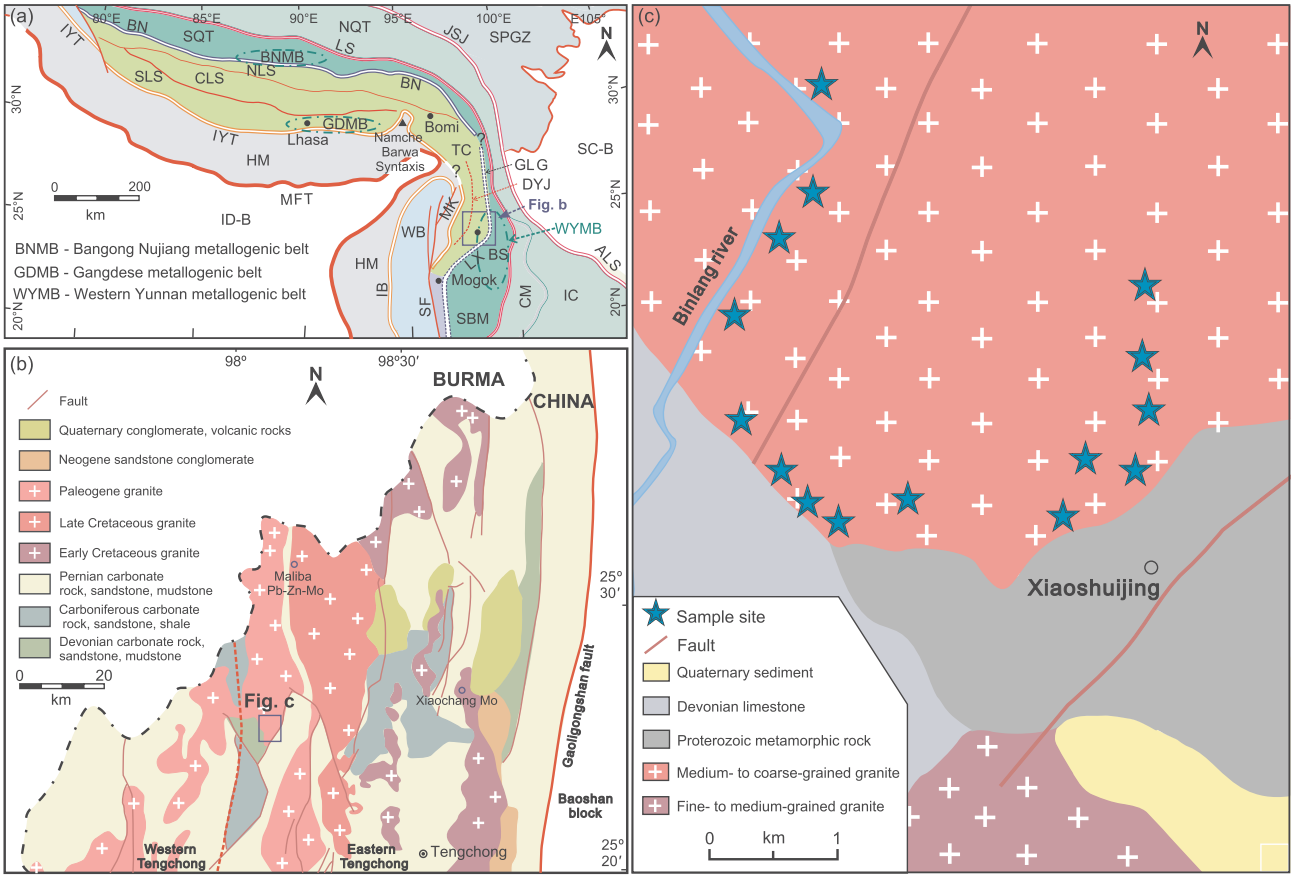

Fig. 1. Generalised maps of: (a) Simplified tectonic map that shows the Tethyan system in the East Cimmerides and West Cathaysides and the locations of the Lhasa Block and Tengchong Block (based on Xu et al., 2015a); (b) simplified geology of the Tengchong Terrane showing major lithological units (modified from Xu et al., 2012); and (c) geology of the Mo-bearing Xiaoshuijing Syenogranite. The Abbreviations are as follows. Palaeo-Tethys: JSJ: Jinshajiang suture; ALS: Ailaoshan suture; LS: Longmu Tso-Shuanghu suture; CM: Changning-Menglian suture; Meso-Tethys: BN: Bangonghu-Nujiang suture; LX: Luxi suture? MK: Myitkyina suture; Neo-Tethys: IYT: Indus-Yarlung-Tsangpo suture; IB: Indo-Burma suture. Blocks and terranes: SC–B, South China Block; ID–B, India Block; SPGZ, Songpan–Ganze terrane; NQT, North Qiangtang terrane; IC, Indochina terrane; SQT, South Qiangtang terrane; BS, Baoshan terrane; SBM, Sibumasu terrane; NLS, North Lhasa terrane; CLS, Central Lhasa terrane; SLS, South Lhasa terrane; TC, Tengchong terrane; WB, West Burma terrane; HM, Himalaya terrane. Faults: MFT, Main frontal thrust fault; SF, Sagaing fault; GLG, Gaoligong fault; DYJ, Dayingjiang Fault.

Of the mineral deposits present in the Tengchong Terrane, molybdenum has been rarely explored for, with only the Xiaochang Mo and Maliba Pb-Zn-Mo deposits known, making the prospectivity of the terrane for Mo uncertain. Chen et al. (2013) report U-Pb zircon ages of 121 ± 1 and 122 ± 1 Ma, and Re-Os Mo ages of 120 ± 2, 125 ± 3 and 125 ± 2 Ma for the Mo-bearing Xiaochang Granite in the Donghe granitic suite and suggest the granite and associated mineralisation were emplaced in a syn-collision setting. Wang et al. (2014b) document a U-Pb zircon age of 79 ± 1 Ma for the granitic host of the Maliba Mo deposit located in the Guyong granitic suite with a Re-Os Mo age of 79 ± 4 Ma and suggest that the granite and mineralisation were emplaced in a subduction-related tectonic setting (Chen et al., 1991; Luo, 1990; Dong et al., 2006; Yang et al., 2009; Deng et al., 2014b; Wang et al., 2014b). The ages of these Mo deposits are coeval with granites indicating that there were two Mo-mineralising events dated at ca. 120 and 80 Ma in the Donghe and Guyong granitic suites (Fig. 1b), but it is acknowledged that these two dates are statistically inadequate, especially given that there are has been no dates on mineralisation in the Binlang River granitic suite until now, which includes the Xiaoshuijing Syenogranite.

This contribution documents field observations, geochemistry, U-Pb zircon and Re-Os Mo dates, and in-situ Hf isotopic data for the Xiaoshuijing Syenogranite and its associated Mo mineralisation. The aim of the study is to gain a better understanding of the petrogenesis of the syenogranite and Mo mineralisation and how they might relate to the other Mo deposits in the Tengchong Terrane.

2. Geological background

The Tengchong Terrane, located in the southern part of eastern Himalayan Orogen, is confined by the Gaoligong Fault to the east and the Myitkyina Suture to the west (Fig. 1a; Qi et al., 2015; Cao et al., 2016). The Indo-Burma Suture is equivalent to the Yarlung-Tsangpo Suture separating rocks related to India to the west from rocks related to the Tengchong (West Burma) Terrane to the east (Fig. 1). The Dayingjiang Fault divides the Tengchong Terrane into the eastern and western parts (Fig. 1b), which have different granites with unique geochemistry, geochronology, zircon Lu–Hf isotopes and metamorphic events (Wang et al., 2006, 2008; Qi et al., 2015).

The oldest units in the Tengchong Terrane are the poorly defined Meso- to Neoproterozoic Gaoligongshan Group consisting of paragneiss and granulite with clastic protoliths (Chen and Xie, 1994). These units are unconformably overlain by a Late Palaeozoic and Early Mesozoic succession of carbonatite and clastic rocks missing Jurassic and Cretaceous units. The Neogene and Quaternary sediments consist of sand, gravel, and continental volcanics (Fig. 1b); Gao et al., 2015.

Mesozoic to Cenozoic granites and related polymetallic mineralisation comprise over 50% of the exposed rocks in the Tengchong Terrane and are included in the Tengchong–Lianghe granitic belt (Xu et al., 2012; Chen et al., 2014; Li et al., 2014; Ma et al., 2014). Based on

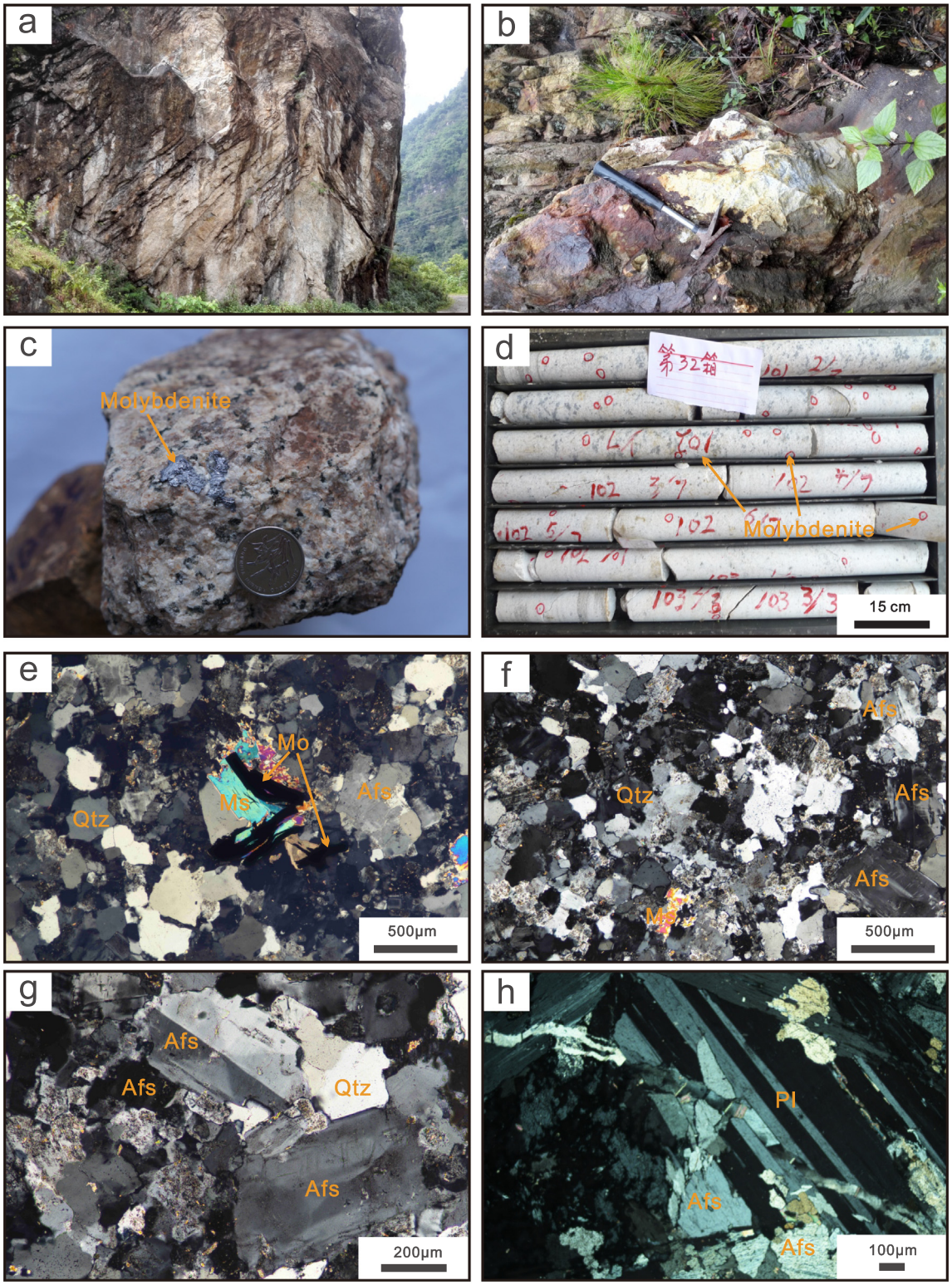

Fig. 2. Petrographical characteristics of the Mo-bearing Xiaoshuijing Syenogranite, Western Yunnan Province. Abbreviations: Afs = alkali feldspar; Qtz = quartz; Pl = plagioclase; Ms = muscovite; Mo = molybdenite.

available data, the Tengchong Terrane has had at least four magmatic episodes represented by: (1) Early Palaeozoic intrusive rocks (Chen et al., 2007; Liu et al., 2009; Dong et al., 2013; Wang et al., 2013; Zhao et al., 2014, 2016); (2) the Early Cretaceous Donghe granitic suite in the eastern part of the terrane (Cong et al., 2011; Xu et al., 2012; Cao et al., 2014; Zhu et al., 2015); (3) the Late Cretaceous Guyong granitic suite in the central and western parts of the terrane (Chen, 1987; Liu et al., 1993; Lu et al., 1993; Xia, 2003; Yang et al., 2009; Jiang et al., 2012); and (4) the Paleogene Binlang River granitic suite that includes the Xiaoshuijing Syenogranite in the western part of the terrane (NRGST, 1985; Shi et al., 1989; Xu et al., 2012; Chen et al., 1991, 2015; Qi et al., 2015).

The Xiaoshuijing Syenogranite was sampled at 25°11′55″N and 98°11′29″E near the Binlang River (Figs. 1, 2). The sample is medium-

Table 1
Major element abundance (in wt%) of the Mo-bearing Xiaoshuijing Syenogranite in the Tengchong Terrane.

Sample No.	HQ-1	HQ-2	HQ-3	HQ-4	HQ-5	HQ-6	HQ-7	HQ-8	HQ-9	HQ-10
XRF-major elements (wt%)										
SiO_2	74.58	73.93	75.2	76.49	74.22	74.66	74.11	73.18	72.04	74.12
Al_2O_3	13.52	13.89	13.15	12.86	13.86	13.82	13.7	15.15	13.81	14.1
Fe_2O_3	1.55	1.68	1.42	0.857	1.67	1.2	1.69	1.32	1.85	1.27
FeO	1.03	1.42	1.26	0.75	0.65	0.6	0.65	0.69	0.85	0.9
MgO	0.272	0.287	0.238	0.241	0.24	0.171	0.265	0.092	0.277	0.251
CaO	1.25	1.2	1.19	1.03	1.13	1.25	1.28	0.291	1.48	1.25
Na_2O	3.12	4.12	3.01	6.74	6.54	7.09	4.7	8.61	3.86	6.69
K_2O	4.95	4.03	5.13	0.404	1.1	0.343	2.93	0.112	4.67	0.844
MnO	0.051	0.037	0.049	0.025	0.03	0.029	0.038	0.014	0.049	0.026
TiO_2	0.129	0.144	0.116	0.119	0.144	0.13	0.147	0.15	0.164	0.132
P_2O_5	0.034	0.034	0.025	0.025	0.035	0.031	0.036	0.02	0.046	0.031
LOI	0.43	0.65	0.46	1.18	1.01	1.25	1.07	1.04	1.71	1.27
Total	100.49	100.77	100.79	99.54	99.62	99.32	99.55	99.63	99.10	99.61
$K_2O + Na_2O$	8.07	8.15	8.14	7.14	7.64	7.43	7.63	8.72	8.53	7.53
K_2O/Na_2O	1.59	0.98	1.70	0.06	0.17	0.05	0.62	0.01	1.21	0.13
A/CNK	1.45	1.49	1.41	1.57	1.58	1.59	1.54	1.68	1.38	1.61
A/NK	1.68	1.70	1.62	1.80	1.81	1.86	1.80	1.74	1.62	1.87
A.R.	3.41	3.35	3.63	3.12	3.08	2.95	3.08	3.60	3.52	2.93
σ	2.06	2.15	2.06	1.52	1.87	1.75	1.87	2.52	2.51	1.82

LOI = loss on ignition. (A.R.) = $[Al_2O_3 + CaO + (Na_2O + K_2O)]/[Al_2O_3 + CaO\text{-}(Na_2O + K_2O)]$ (wt%), (σ) = $(Na_2O + K_2O)^2/(SiO_2\text{-}43)$ (wt%).

to coarse-grained, equigranular, pale red in colour, and consists of alkali feldspar (50–55%), plagioclase (20–25%), quartz (20–25%), muscovite (< 1%), opaques minerals (< 1%), and trace amounts of apatite, allanite, and zircon, which is a mineral assemblage characteristic of a syenogranite. The alkali feldspar is microcline, subhedral measuring 2–10 mm long, and has cross-hatched twinning (Fig. 2e, f, g). The plagioclase feldspar is andesine (Fig. 2h), 1–4 mm long, and has oscillatory zoning and is variable sericitised. The quartz is 1–5 mm across, granular and commonly mixed with alkali feldspar and plagioclase. Molybdenite, when present, commonly has a grain size of 15–20 mm, a bladed or flaky habit, and is disseminated in the syenogranite to a depth greater than 200 m being the vertical extent of the drilling (Fig. 2c, d).

3. Analytical methods

Fifteen fresh samples of the Xiaoshuijing Syenogranite were analysed for major and trace elements. One of these samples was U-Pb zircon dated and analysed for Hf isotopes, and four samples of molybdenite were Re-Os dated. The analyses were performed using the X-ray Fluorescence (XRF) and Laser Ablation-Inductively Coupled Plasma-Mass Spectrometry (LA-ICP-MS) in the Analytical Laboratory at the Beijing Research Institute of Uranium Geology (c.f. Zhang et al., 2012, Zou et al., 2017). Major element compositions were determined using a SHIMADZU XRF-1800 sequential XRF spectrometer with an error estimate of < ± 5%. Trace elements were analysed using a Thermo-Scientific X Series II ICP-MS, with an estimate error of less than ± 8%. A 50 mg aliquot of powder from each sample was dissolved in a high-pressure Teflon bomb using a HCl + HF + HNO_3 + $HClO_4$ mixture. An internal standard solution containing single element Rh was used for monitoring signal drift during ion counting. The USGS standard GSP-2 and Chinese National standards GSR-1 and GSR-2 were used for calibration of element concentrations in the unknowns. During analysis, data quality was monitored by repeated analyses of rock reference materials, together with regular monitoring of total procedural blanks.

U–Pb dating and trace element analyses of zircon were conducted at the LA-ICP-MS microanalysis laboratory affiliated with the State Key Laboratory of Geological Processes and Mineral Resources, China University of Geosciences, Beijing (c.f. Cao et al., 2016; Zhang et al., 2012). The spot sizes of the laser ablation analyses were 35 μm in diameter for the U-Pb zircon dates and 50 μm for the Hf isotopes analyses. The TEMORA standard zircon was selected as the standard for U-Pb dating and analysed twice every 5 analyses of the zircons with unknown dates. The common lead correction was carried using the EXCEL program ComPbCorr#3 15G (Andersen, 2002). NIST612 was the external standard for the elemental compositions, and Si was the internal standard. The geochronological data were processed using the ICP-MS Data Cal software documented by Liu et al. (2010) and Isoplot by Ludwig (2012). The accuracy of the individual LA-ICP-MS analyses are quoted at the 95% or 2σ confidence level.

Some of the dated zircons were analysed for Lu-Hf isotopes in the same or adjacent areas using the LA-MC-ICP-MS at the Laboratory of Continental Tectonics and Dynamics, Chinese Academy of Geological Sciences. The instruments used in the experiment were the Thermo-Finnigan Neptune MC-ICP-MS and Coherent UP193 ultraviolet laser ablation system. Helium was used as the carrier gas. The ablating diameter was 44 μm and the analyses were monitored using the standard GJ-1 zircon (Geng et al., 2011). The zircon standard has a $^{176}Hf/^{177}Hf$ ratio of 0.281988 ± 18 and $^{176}Lu/^{177}Hf$ ratio of 0.0003 (Morel et al., 2008).

The Re-Os molybdenite isotope ratios were measured using a TJA X-series ICP-MS at the National Research Centre for Geoanalysis, Chinese Academy of Geological Sciences in Beijing. The standard material for the analysis is GBWO04435 (JDC) with a date of 141 ± 1.9 Ma. The Re and Os chemical separation procedures and mass spectrometer analyses followed those of Smoliar et al. (1996). The data were processed also using Isoplot (Ludwig, 2012).

4. Analytical results

4.1. Geochemical characteristics of the Xiaoshuijing Syenogranite

Whole-rock major and trace element data for the granitic samples are listed in Tables 1 and 2. The alkaline ($Na_2O + K_2O$) values vary from 7.14 to 8.72%, and the K_2O/Na_2O ratio varies from 0.01 to 1.59. The Alkalinity Ratio index (AR) is 2.93–3.63 and Rittmann Index ($\sigma = (Na_2O + K_2O)^2/(SiO_2 - 43)$) is 1.52–2.52, characteristic of high-K, alkaline affinities for the syenogranite.

The aluminium saturation index (A/CNK) is a measure of whether there is an excess in, or lack of, Al. If there is an excess of Al required to form feldspars, the granite is peraluminous, rocks with a lack of Al_2O_3 are termed metaluminous, and those that are oversaturated in $Na_2O + K_2O$ and undersaturated in Al_2O_3 are peralkaline. The A/CNK value for the Xiaoshuijing Syenogranite is 1.38–1.68, and the A/NK

Table 2
Trace elements assays (ppm) of the Mo-bearing Xiaoshuijing Syenogranite in the Tengchong Terrane.

Sample No.	HQ-1	HQ-2	HQ-3	HQ-4	HQ-5	HQ-6	HQ-7	HQ-8	HQ-9	HQ-10	HQ-11	HQ-12	HQ-13	HQ-14	HQ-15
ICP-MS-Trace element (ppm)															
Li	45.8	10.4	29.1	7.64	7.69	7.84	8.06	1.21	14.7	8.8	6.53	17.9	37.5	24.2	17.6
Be	3.33	3.24	3.8	3.95	2.72	5.03	2.59	3.4	3.76	3.77	3.36	2.42	3.09	2.63	3.63
Sc	2.35	2.7	1.98	2.27	2.59	2.17	2.04	1.81	2.65	2.61	2.47	2.44	2.18	2.21	1.34
V	8.21	8.17	7.04	7.83	9.78	8.87	9.2	5.75	11.1	8.49	9.86	9.13	7.88	10.1	7.02
Cr	1.01	0.825	0.647	1.3	1.01	0.937	1.14	0.949	1.14	0.876	0.784	1.02	0.686	0.856	0.783
Co	1.26	1.37	1.14	1.53	1.06	0.453	1.56	0.591	1.84	1.46	1.34	1.3	1.2	1.49	0.703
Ni	0.689	0.669	0.508	0.495	0.581	0.479	0.767	0.305	0.734	0.539	0.575	0.544	0.497	0.542	0.465
Cu	0.882	0.888	0.745	0.726	0.876	0.821	0.931	2.39	0.99	1.06	0.923	0.817	0.711	1.01	0.555
Zn	26.5	27.5	31.6	21.4	23.2	15.6	28.1	10.7	38.7	23.8	31	31.7	27.4	27.4	17.4
Ga	16.3	17.6	15.1	14	15.6	15.8	16.1	17.5	15.9	17.3	17.1	16.3	16.4	16.1	15
Rb	289	233	280	39	65	21.1	160	5.11	235	62.4	289	278	285	269	195
Sr	85.7	90.7	78.8	311	91.6	247	102	152	137	134	98.6	86.3	90.8	91.1	56.3
Y	37.7	30.4	22.5	28.5	27.8	26.4	29	19.1	33.8	22.6	30.5	25.1	42.8	23.7	37.9
Nb	18	19.7	16.3	14.3	19	18.3	17	22.3	21.9	16.1	17.3	14.7	17.2	16.1	14
Mo	0.917	0.656	0.48	0.357	0.309	0.046	0.624	0.352	0.503	0.213	0.621	0.237	0.59	0.067	0.537
Cd	0.203	0.141	0.113	0.111	0.134	0.034	0.098	0.067	0.087	0.164	0.135	0.034	0.095	0.155	0.052
In	0.026	0.023	0.03	0.027	0.028	0.035	0.016	0.05	0.044	0.031	0.034	0.029	0.025	0.018	0.013
Sb	0.043	0.106	0.188	0.111	0.066	0.075	0.043	0.798	0.122	0.597	0.041	0.029	0.014	0.02	0.019
Cs	6.23	4.8	6.43	2.5	1.77	0.985	3.38	0.492	4.38	3.28	6.09	7.05	6.27	7.04	4.34
Ba	203	174	240	69.5	184	149	173	29.3	254	817	238	199	241	227	69.2
Ta	1.94	2.2	2.92	2.59	2.19	2.12	2	2.85	2.42	2.56	2.17	1.76	2.09	1.87	2.04
W	0.589	0.74	0.379	2.79	0.425	0.601	0.583	0.573	0.385	0.436	0.535	0.295	0.55	0.406	0.278
Tl	1.19	1.07	1.27	0.259	0.288	0.107	0.816	0.047	1.12	0.315	1.46	1.48	1.25	1.16	0.992
Pb	37.1	37.4	41.7	14	27.1	16.5	32.4	13.4	39	18.3	41	38.4	38.1	35.5	30.5
Bi	0.063	0.101	0.08	0.03	0.163	0.128	0.115	0.443	0.332	0.268	0.179	0.096	0.057	0.107	0.024
Th	37.5	43.7	33.5	34.1	31.7	35.7	43.7	44.2	39.2	39.5	33.8	38.3	37	44.2	16.9
U	12.5	13.8	11.2	5.85	8.1	7.3	7.69	6.72	8.12	7.37	7.86	8.66	8.79	9.14	6.81
Zr	37.1	31.1	25.2	24.8	27.1	37.4	42.2	47.1	38	17.1	40.8	40.2	44.7	36.8	19.5
Hf	1.76	1.46	1.14	1.12	1.41	1.94	2.25	2.13	1.73	0.984	1.67	1.72	2.15	1.55	1.13
La	26.7	34.6	19.5	31.8	28.7	30.9	31.9	35.7	31.9	29.7	29.7	27.1	28.8	36.8	10
Ce	50.6	65.7	36.9	59.3	53.9	57.4	60.4	68.4	59.4	56.3	56.1	51.2	55	68.2	19.8
Pr	5.82	7.45	4.24	6.64	6.14	6.39	6.89	7.6	6.72	6.52	6.36	5.79	6.24	7.52	2.42
Nd	21.5	26.6	15.5	23.8	22.3	23.1	24.5	26.9	24.3	23.8	22.7	21.2	22.9	26.4	10
Sm	4.81	5.46	3.3	4.59	4.74	4.69	5	4.61	5.08	4.67	4.81	4.23	5.15	4.82	3.05
Eu	0.478	0.471	0.443	0.427	0.483	0.498	0.451	0.405	0.593	0.414	0.528	0.516	0.526	0.521	0.327
Gd	4.73	4.55	2.53	4.16	3.87	4.15	4.5	3.58	4.92	3.73	4.29	3.67	5.14	3.89	3.68
Tb	1.01	0.843	0.612	0.782	0.807	0.767	0.816	0.564	0.98	0.676	0.903	0.762	1.1	0.79	0.921
Dy	6.71	4.87	3.25	4.37	4.48	4.1	4.68	3.06	5.27	3.18	4.76	3.88	6.64	3.61	5.94
Ho	1.24	0.889	0.708	0.848	0.863	0.782	0.97	0.635	1.03	0.748	1.02	0.771	1.31	0.714	1.24
Er	3.61	2.75	2.13	2.61	2.73	2.62	2.79	1.89	3.45	1.88	2.74	2.37	4.52	2.15	3.87
Tm	0.67	0.546	0.408	0.464	0.541	0.483	0.658	0.467	0.602	0.381	0.573	0.418	0.789	0.45	0.655
Yb	4.29	3.24	3.18	3.53	3.62	3.51	3.65	2.96	4	3.16	3.37	2.82	5.23	2.44	4.65
Lu	0.634	0.448	0.344	0.446	0.464	0.418	0.455	0.412	0.486	0.45	0.495	0.348	0.693	0.415	0.618
ΣREE	132.80	158.42	93.05	143.77	133.64	139.81	147.66	157.18	148.73	135.61	138.35	125.08	144.04	158.72	67.17
LREE	109.91	140.28	79.88	126.56	116.26	122.98	129.14	143.62	127.99	121.40	120.20	110.04	118.62	144.26	45.60
HREE	22.89	18.14	13.16	17.21	17.38	16.83	18.52	13.57	20.74	14.21	18.15	15.04	25.42	14.46	21.57
LREE/HREE	4.80	7.73	6.07	7.35	6.69	7.31	6.97	10.58	6.17	8.55	6.62	7.32	4.67	9.98	2.11
La_N/Yb_N	4.21	7.22	4.14	6.09	5.36	5.95	5.91	8.15	5.39	6.35	5.96	6.49	3.72	10.19	1.45
δEu	0.31	0.38	0.47	0.3	0.34	0.34	0.29	0.3	0.36	0.3	0.36	0.40	0.31	0.37	0.3
δCe	0.95	0.96	0.95	0.96	0.95	0.96	0.95	0.97	0.95	0.95	0.96	0.96	0.96	0.96	0.94

La_N/Yb_N values are La/Yb ratios normalized to chondrite values after McDonough and Sun (1995), $Eu/Eu^* = 2*w(Eu)_N/[w(Sm)_N + w(Gd)_N]$, $Ce/Ce^* = 2*w(Ce)_N/[w(La)_N + w(Pr)_N]$.

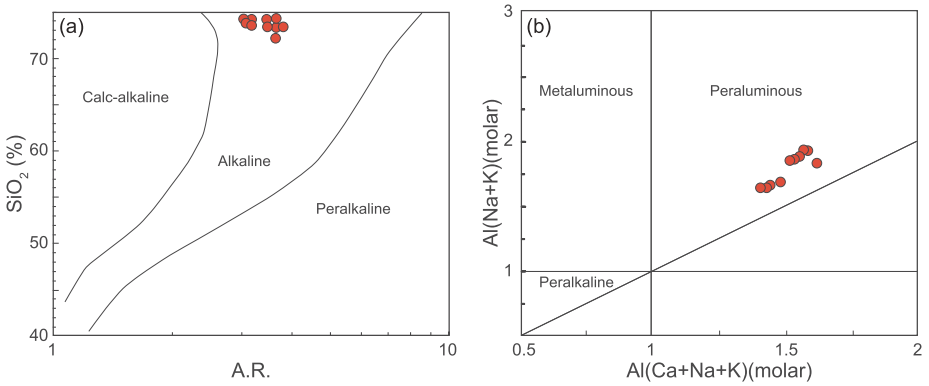

Fig. 3. Discrimination diagrams for the Mo-mineralised Xiaoshuijing Syenogranite in the Tengchong Terrane: (a) SiO_2 vs A.R. diagram (after Wright, 1969); and (b) A/NK vs A/CNK discrimination diagram (after Maniar and Piccoli, 1989).

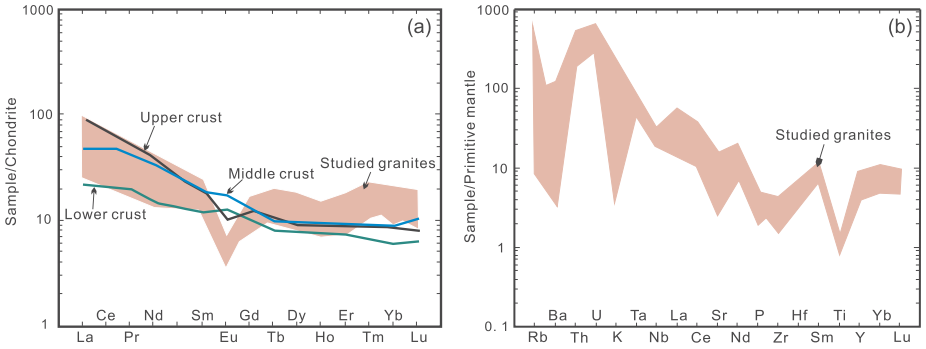

Fig. 4. Diagrams showing: (a) Chondrite-normalised REE patterns; (b) Primitive mantle-normalised trace element patterns for the Mo-mineralised Xiaoshuijing Syenogranite. The normalised data is after McDonough and Sun (1995). The REE contents of the lower, middle and upper crust are from Rudnick and Fountain (1995).

Table 3
Zircon trace elements from the Mo-bearing Xiaoshuijing Syenogranite in the Tengchong Terrane.

Spot No.	La	Ce	Pr	Nd	Sm	Eu	Gd	Tb	Dy	Ho	Er	Tm	Yb	Lu	Y
XSJ-03-01	0.01	14.27	0.05	1.56	3.98	0.14	25.86	9.01	112.94	44.26	207.33	47.77	476.13	74.96	1214.55
XSJ-03-02	0.57	23.99	0.41	3.18	5.99	0.85	24.07	8.30	99.32	40.10	194.82	46.59	487.27	87.18	1214.95
XSJ-03-03	0.03	9.49	0.02	0.14	1.41	0.13	9.05	3.06	52.32	20.93	113.07	29.42	322.07	60.8	667.94
XSJ-03-04	2.59	49.25	1.19	10.59	12.90	2.44	58.98	20.86	253.02	95.33	409.53	96.93	982.12	143.77	2614.96
XSJ-03-05	0.01	1.66	0.12	2.41	16.63	1.92	184.71	90.20	990.07	257.33	794.57	136.25	1035.71	128.16	7635.1
XSJ-03-06	1.58	17.95	0.62	2.45	3.27	0.49	23.44	11.03	141.84	59.83	287.12	72.30	762.7	123.48	1747.34
XSJ-03-07	0.2	21.93	0.17	1.90	6.67	0.15	64.71	29.71	427.19	174.76	846.03	213.14	2118.8	338.58	5179.09
XSJ-03-08	1.48	10.38	0.57	3.67	3.44	0.74	19.30	5.59	59.46	26.28	113.78	30.04	313.28	51.08	792.79
XSJ-03-09	6	32.89	2.74	10.87	8.17	0.45	35.7	13.2	171.17	65.92	319.24	78.57	787.85	121.33	1936.28
XSJ-03-10	1.34	17.37	1.11	6.92	6.56	0.47	23.56	7.70	97.02	37.78	187.35	47.63	517.44	84.43	1173.20
XSJ-03-11	0.01	0.61	0.03	0.68	5.06	0.16	39.71	20.73	280.59	97.81	401.02	86.83	807.41	109.68	3011.91
XSJ-03-12	0.01	19.08	0.01	0.01	3.67	1.00	35.68	10.30	132.16	56.61	271.03	64.91	671.62	118.97	1640.39
XSJ-03-13	0.01	17.79	0.01	0.89	1.35	0.39	11.92	5.64	71.14	29.18	150.90	38.46	410.96	70.9	942.57
XSJ-03-14	0.05	6.19	0.08	2.59	4.33	0.56	30.79	12.09	150.54	64.37	302.78	72.01	688.72	119.34	1914.35
XSJ-03-15	1.73	34.56	1.30	8.78	8.32	0.7	32.51	12.35	155.60	61.63	300.62	71.33	705.24	133.93	1895.12
XSJ-03-17	0.07	15.52	0.03	0.69	3.45	0.55	18.36	7.07	81.35	36.38	156.75	35.33	368.18	67.11	1053.74
XSJ-03-18	0.03	42.05	0.08	1.40	3.44	1.14	22.77	8.55	114.39	47.29	236.66	59.87	641.11	117.32	1478.86
XSJ-03-19	0.11	37.43	0.18	2.39	7.19	1.67	32.11	12.46	151.78	60.6	287.82	72.47	771.57	130.27	1757.43
XSJ-03-20	0.01	16.96	0.13	1.46	5.66	0.57	35.34	14.61	197.79	78.19	379.35	95.54	1003.12	156.84	2240.31

Spot No.	Ti	Nb	Hf	Ta	Pb	Th	U	ΣREE	LREE/HREE	Eu/Eu*	Ce/Ce*	$(Nb/Pb)_N$	$T_{Ti\text{-}in\text{-}zirc}$ (°C)
XSJ-03-01	3.4	10.2	13136.7	8.6	3.3	400	796.9	1018.27	0.020	0.03	87.56	30.68	671
XSJ-03-02	2	4.0	12070.6	2.6	1.3	434.3	515.4	1022.63	0.035	0.19	11.44	30.51	631
XSJ-03-03	/	4.1	13259.3	3	/	239	588.3	621.93	0.018	0.08	106.99	/	/
XSJ-03-04	1.9	6.0	11196.7	3.1	1.6	1499.8	1146	2139.49	0.038	0.23	6.77	36.74	625
XSJ-03-05	9.7	10.3	13143.7	6.7	0.7	178.6	6208.3	3639.76	0.006	0.07	4.06	158.2	764
XSJ-03-06	5.7	18.2	12832.1	10.9	4.7	833.8	2073.2	1508.1	0.018	0.12	4.38	38.95	714
XSJ-03-07	0.8	85.3	17009.8	59.4	/	2925.5	2655.8	4243.96	0.007	0.01	26.7	/	569
XSJ-03-08	/	3.8	12130.6	2.6	/	185.9	371.2	639.1	0.033	0.22	2.75	/	/
XSJ-03-09	7.5	12.4	13,288	8.4	/	842.4	1619	1654.1	0.038	0.07	1.96	/	739
XSJ-03-10	4.5	7.6	13940.1	5.3	/	519.3	1191.5	1036.69	0.034	0.1	3.21	/	693
XSJ-03-11	5.4	1.3	15014.9	2	1.1	89.7	1109.7	1850.31	0.004	0.03	5.5	11.83	709
XSJ-03-12	/	3.7	11,003	3.1	8.1	473.4	564.0	1385.03	0.017	0.17	/	4.66	/
XSJ-03-13	/	6.6	15,271	2.8	3.6	326.1	680.4	809.53	0.026	0.2	/	18.76	/
XSJ-03-14	18.2	3.2	13067.3	1.3	2.4	229	381.8	1454.42	0.01	0.11	19.03	12.98	829
XSJ-03-15	1.8	9.8	18810.8	6.4	2.0	1419.3	1351.2	1528.6	0.038	0.11	5.29	48.38	622
XSJ-03-17	2.6	2.9	15511.3	1.6	7.9	265	426.9	790.85	0.026	0.17	87.5	3.71	649
XSJ-03-18	3.6	8.6	18139.8	5.3	2.4	1119.5	1182.2	1296.1	0.039	0.29	141.98	35.53	675
XSJ-03-19	7.3	4.8	14162.9	2.4	0.9	530.4	539.7	1568.04	0.032	0.28	50.55	54.47	737
XSJ-03-20	3.2	9.2	18424.8	7.2	/	866.5	1783.7	1985.57	0.013	0.09	39.33	/	665

Notes: /: below the limit of determination; $Ce/Ce^* = CeN/(La_N{*}Pr_N)^{0.5}$; $Eu/Eu^* = Eu_N/(Sm_N{*}Gd_N)^{0.5}$; N denotes normalization using chondrite values after Sun and McDonough (1989); T Ti-in-zrc: Ti-in-zircon crystallization temperatures at $\alpha TiO_2 = 0.7$ (Clairborne et al., 2006; Ferry and Watson, 2007).

value is 1.62–1.87, indicating that the syenogranite is peraluminous (Fig. 3).

The Xiaoshuijing Syenogranite has a high total REE (ΣREE) of 93.05–158.72 ppm, light REE (LREE) to heavy REE (HREE) ratio of 2.11–8.55, and $(La/Yb)_N$ value of 1.45–10.19. The Chondrite-normalised REE patterns are enriched in LREE, and the samples have a strong negative Eu-anomaly (Eu/Eu* = 0.29–0.47; Table 2; Fig. 4a). These data are characteristic of a middle to upper crustal source for the syenogranite (Rudnick and Fountain, 1995). The trace element spider diagrams for the syenogranite are relative enriched in the large ion lithophile elements (LILE) Rb, Th, U and Pb, and depleted in Ba, Sr, P, Ti and Eu, and the high field strength elements (HFSE) Zr and Hf (Fig. 4b). The high Rb, and low Ba and Sr values are indicative of the fractional crystallisation of orthoclase and plagioclase, and the Eu depletion is indicative of plagioclase fractionation. The transitional mantle incompatible elements Cr and Ni contents are low and show that the syenogranite has a minimal input from deeper sources precluding it from having a mantle component.

4.2. Zircon trace elements

Zircon trace elements are sensitive monitors of the composition and

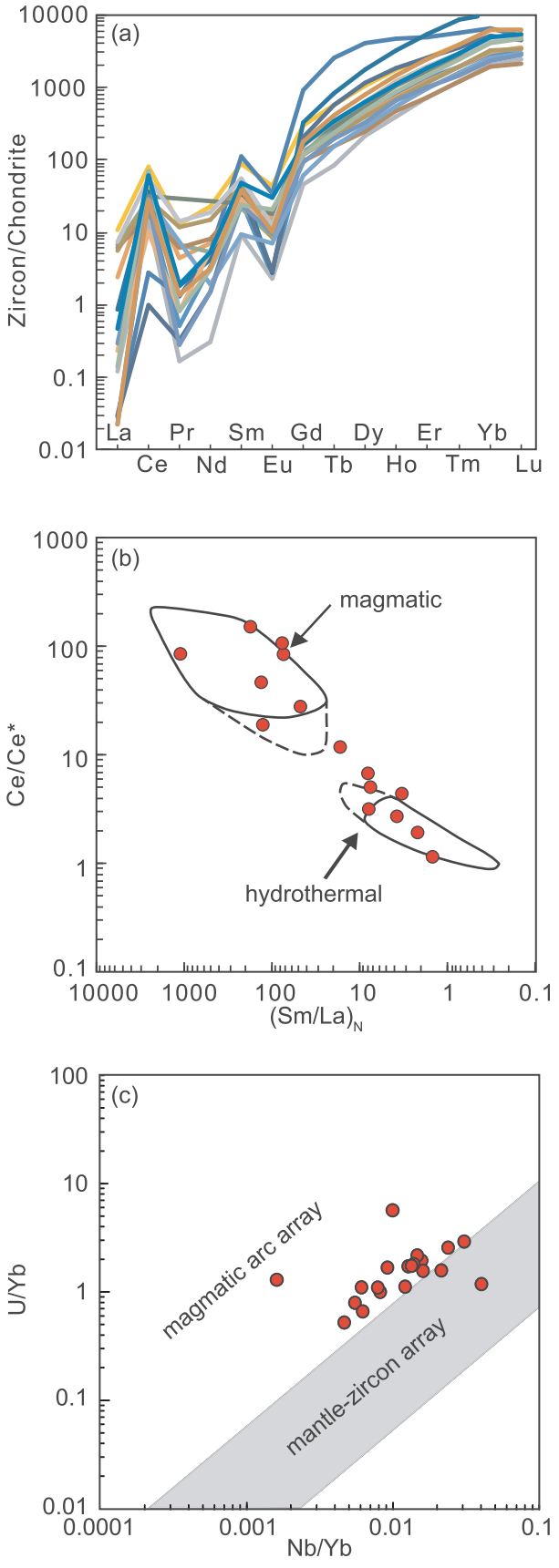

Fig. 5. Diagrams showing: (a) Chondrite-normalised REE patterns; (b) Ce/Ce* vs $(Sm/La)_N$ (N denotes Chondrite normalised values from Hoskin, 2005); and (c) $\log_{10}$ Nb/Yb vs $\log_{10}$ U/Yb diagrams showing the origin of the zircon grains in the Xiaoshuijing Syenogranite (after Grimes et al., 2015).

temperature of their parental magma (Grimes et al., 2015). The trace element content of zircons from the Xiaoshuijing Syenogranite have a fractionated Chondrite-normalised REE pattern with a positive Ce anomaly (Ce/Ce* of 1.96–141.98) and negative Eu anomaly (Eu/Eu* of 0.01–0.29), which are characteristic of magmatic zircons (Table 3; Fig. 5a, b; Hoskin and Schaltegger, 2003; Whitehouse and Platt, 2003). The Ce enrichment is probably related to an increased oxygen fugacity or decreasing temperature (Trail et al., 2012). The presence of the negative Eu anomaly is characteristic of plagioclase crystallisation earlier than the crystallisation of the zircons (Hoskin and Schaltegger, 2003). The zircons also assay 371–2656 ppm U, 90–2926 ppm Th, 1.3–85 ppm Nb, 313–2119 ppm Yb and 1.8–18 ppm Ti, with Th/U ratios of 0.03–1.31, Nb/Yb ratios of 0.002–0.04, and U/Yb ratios of 0.55–5.99 (Fig. 5c). The U/Yb ratios for these zircons are indicative of a continental-arc setting (Grimes et al., 2015). The syenogranite's estimated temperature of crystallisation based Ti thermometry vary from at least 569° to 829 °C (Watson et al., 2006; Clairborne et al., 2006; Ferry and Watson, 2007).

4.3. U-Pb zircon dating

The U-Pb zircon analyses for sample XSJ-03 from the Xiaoshuijing Syenogranite are included in Table 4. The zircons are euhedral, elongate or columnar (Fig. 6). Nineteen spots were measured on 19 zircon grains that have clear oscillatory zoning on cathodoluminescence (CL) images, and are characteristic of a magmatic origin (Rubatto, 2002).

Three inherited zircon grains gave ages of 198, 375, and 668 Ma. The other spots gave similar ages, with the $^{206}Pb/^{238}U$ ages ranging from 62 to 71 Ma, and all plot on or near the U-Pb age Concordia diagram (Fig. 7). The analyses yield a weighted mean age of 65 ± 1 Ma (n = 14, MSWD = 2.1), which is interpreted as the crystallisation age of the syenogranite.

4.4. Zircon Lu-Hf isotopes

The Hf isotopes measured on the dated zircons from sample XSJ-03 are given in Table 5. The zircons have an average high $^{176}Hf/^{177}Hf$ ratio of 0.2823 and average low $^{176}Lu/^{177}Hf$ ratio of 0.0011. The very low radiogenic Hf concentrations are indicative of zircons crystallising from a magma (Amelin et al., 2000). The $\varepsilon_{Hf}(t)$ values are negative, ranging from −18.23 to −12.92, corresponding to a crustal source for the magma. The associated T_{DM}^1 model ages vary from 1427 to 1226 Ma, and the T_{DM}^2 model ages vary from 2281 to 1950 Ma, indicative of a Palaeoproterozoic crustal source.

4.5. Molybdenite Re-Os dating

The Re-Os Mo analyses for four samples of the Xiaoshuijing Syenogranite are presented in Table 6. The model ages are between 65 ± 1 and 66 ± 1 Ma, with a weighted mean age of 65 ± 1 Ma (MSWD = 2.6). The ^{187}Re-^{187}Os diagram shows a linear distribution yielding a well-defined isochron age of 64 ± 2 Ma (Fig. 8), which is interpreted at the age of the Mo mineralisation.

5. Discussion

5.1. Genetic type

The Xiaoshuijing Syenogranite samples plot in the combined I- and S-type granite fields on the Y vs 10,000 Ga/Al, Nb vs 10,000 Ga/Al, FeO_T vs MgO-Zr + Nb + Ce + Y, and $(Na_2O + Na_2O)$ vs CaO-Zr + Nb + Ce + Y discrimination diagrams in Fig. 9a–d (after Collins et al., 1982; Whalen et al., 1987). In addition, the samples lack arfvedsonite and riebeckite, which are minerals characteristic of A-type granites (Collins et al., 1982; Whalen et al., 1987). These features indicate that the syenogranite is not an A-type granite.

Table 4
Laser Ablation–Inductively Coupled Plasma–Mass Spectrometry (LA-ICP-MS) U–Pb data from the Mo-bearing Xiaoshuijing Syenogranite in the Tengchong Terrane.

Spot No.	Content (ppm)				Isotopic rations						Age (Ma)					
	Pb_c	U	Th	Th/U	$^{207}Pb/^{206}Pb$	1σ	$^{207}Pb/^{235}U$	1σ	$^{206}Pb/^{238}U$	1σ	$^{207}Pb/^{206}Pb$	1σ	$^{207}Pb/^{235}U$	1σ	$^{206}Pb/^{238}U$	1σ
1	59	797	400	0.50	0.0576	0.0013	0.4794	0.0132	0.0599	0.0010	517	41.7	398	9	375	6.1
2	7	515	434	0.84	0.0504	0.0079	0.0679	0.01	0.0099	0.0006	213	329.6	67	9.6	64	3.6
3	7	588	239	0.41	0.0476	0.006	0.0640	0.0078	0.0098	0.0003	80	274	63	7.5	63	1.7
4	17	1146	1499	1.31	0.0489	0.0079	0.0664	0.0105	0.01	0.0004	143	340.7	65	10	64	2.7
5	209	6208	179	0.03	0.051	0.0009	0.2203	0.0041	0.0312	0.0003	239	42.6	202	3.4	198	1.9
6	25	2073	833	0.4	0.0501	0.0037	0.0726	0.0055	0.0104	0.0003	211	170.3	71	5.2	67	2.1
8	6	371	186	0.5	0.1687	0.0223	0.2471	0.0272	0.011	0.001	2546	222.4	224	22.1	71	6.3
9	20	1619	842	0.52	0.0498	0.0031	0.0715	0.0043	0.0104	0.0002	187	142.6	70	4.1	67	1
10	15	1192	519	0.44	0.0481	0.0037	0.0693	0.005	0.0105	0.0002	106	170.3	68	4.8	68	1.5
11	127	1110	90	0.08	0.0654	0.0017	0.9877	0.0262	0.1092	0.0017	787	48	698	13.4	668	10.1
12	8	564	473	0.84	0.073	0.0304	0.1114	0.0483	0.0105	0.0013	1017	670.7	107	44.1	67	8.2
13	8	680	326	0.48	0.0493	0.0058	0.0689	0.0074	0.0105	0.0005	161	255.5	68	7.1	67	3.1
14	4	382	229	0.6	0.0529	0.0072	0.0672	0.007	0.0101	0.0006	324	281.4	66	6.6	64	3.7
15	19	1351	1419	1.05	0.0489	0.0045	0.0719	0.0073	0.0105	0.0003	143	200	71	6.9	68	1.6
16	47	4371	1386	0.32	0.0480	0.0016	0.0638	0.0018	0.0097	0.0001	98	75.9	63	1.7	62	0.8
17	5	427	264	0.62	0.0535	0.015	0.0717	0.0176	0.0104	0.0006	350	533.3	70	16.7	67	4
18	15	1182	1119	0.95	0.0487	0.0025	0.065	0.0034	0.0099	0.0002	132	−75	64	3.2	63	1.1
19	7	540	530	0.98	0.0544	0.0046	0.0709	0.006	0.0099	0.0004	387	192.6	70	5.7	63	2.5
20	21	1784	866	0.49	0.0509	0.0022	0.071	0.0028	0.0103	0.0002	235	100.0	70	2.6	66	1.4

Error in Standard calibration was 0.16% (not included in above errors but required when comparing data from different mounts).

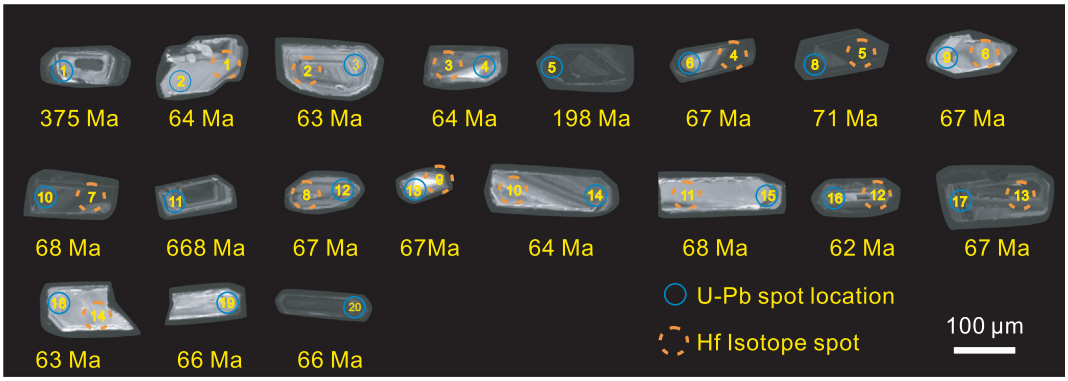

Fig. 6. Cathodoluminescence (CL) images of zircons for the Mo-bearing Xiaoshuijing Syenogranite and locations of U–Pb dated and Hf isotope analysed spots.

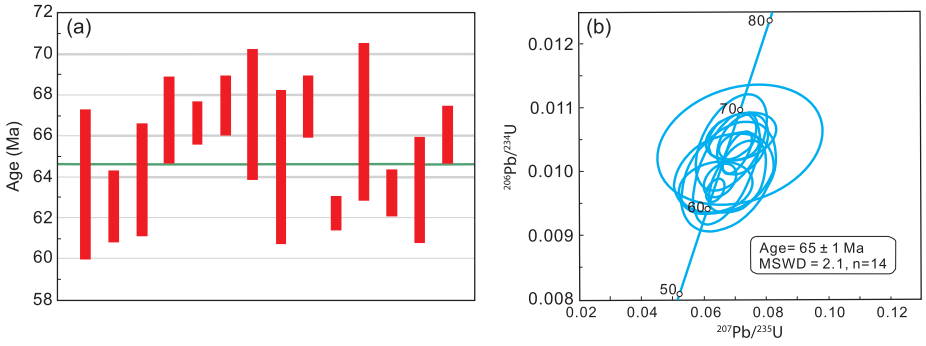

Fig. 7. U-Pb zircon concordia plots for the Mo-mineralised Xiaoshuijing Syenogranite in the Tengchong Terrane.

I-type granites contain hornblende and biotite, and S-type granites are characterised by andalusite, cordierite, garnet, and muscovite (Chappell and White, 1992). The Xiaoshuijing Syenogranite does not contain hornblende common in I-type granites, and andalusite, cordierite, garnet, or muscovite common in S-type granites (Chappell and White, 1974, 1992). This means that the syenogranite is not an S-type granite, because it lacks Al-rich minerals, even though it is peraluminous. The ($Na_2O + Na_2O$) vs CaO-Zr + Nb + Ce + Y plot in Fig. 9d shows that the syenogranite is a fractionated granite, confirmed by its high Rb, low Ba and Sr values, and negative Eu anomaly. The syenogranite is thus derived from a mafic and metaluminous source through fractional crystallisation making it an I-type granite according to the petrological criteria of Chappell and White (1974) (c.f. Lee and Morton, 2015). Fractionated granitic magmas are easily contaminated by country rocks due to their relatively prolonged crystallisation time. Thus, fractionated granites do not always reflect the nature of their source and the chemistry of the primary magma (e.g. Wu et al., 2017). The consequence of this is that the geochemical-based I- and S-type classification for the Xiaoshuijing Syenogranite cannot be applied. Furthermore, the conflicting geochemical characteristics for I- and S-type granites highlight the difficulty of using this classification for fractionated granites and questions the necessity of this classification.

Table 5
Lu-Hf isotope compositions of zircon of Sample XSJ-03 from the Mo-bearing Xiaoshuijing Syenogranite in the Tengchong Terrane.

Spot No.	T(Ma)	$^{176}Yb/^{177}Hf$	2σ	$^{176}Lu/^{177}Hf$	2σ	$^{176}Hf/^{177}Hf$	2σ	ε_{Hf} (0)	ε_{Hf} (t)	T_{Hf1}(Ma)	T_{Hf2}(Ma)	$f_{Lu/Hf}$
1	64	0.027934	0.003406	0.001055	0.000096	0.282313	0.000028	−16.23	−14.87	1327	2071	−0.97
2	63	0.028881	0.000481	0.001147	0.00001	0.282332	0.000025	−15.57	−14.24	1304	2030	−0.97
3	64	0.001595	0.00006	0.000055	0.000002	0.282362	0.000026	−14.51	−13.11	1226	1960	−0.99
4	67	0.038024	0.000352	0.001371	0.000003	0.282367	0.00003	−14.33	−12.92	1262	1950	−0.96
5	71	0.052662	0.001131	0.002006	0.000024	0.282330	0.000027	−15.63	−14.16	1337	2032	−0.94
6	67	0.035497	0.000220	0.001361	0.000025	0.282352	0.000027	−14.84	−13.43	1283	1984	−0.96
7	68	0.027174	0.000671	0.001069	0.000015	0.282308	0.000027	−16.41	−14.97	1335	2080	−0.97
8	67	0.03494	0.000476	0.001339	0.000013	0.282303	0.000025	−16.60	−15.19	1351	2093	−0.96
9	67	0.037791	0.000516	0.001109	0.000018	0.282243	0.000028	−18.72	−17.30	1427	2225	−0.97
10	64	0.027946	0.000790	0.001031	0.000018	0.282307	0.000025	−16.43	−15.07	1335	2085	−0.97
12	62	0.027528	0.000075	0.000957	0.000003	0.282219	0.000022	−19.55	−18.23	1455	2281	−0.97
13	67	0.036916	0.000093	0.001329	0.000003	0.282307	0.000023	−16.43	−15.02	1345	2084	−0.96
14	63	0.02964	0.000488	0.00109	0.000026	0.282261	0.000021	−18.08	−16.74	1401	2188	−0.97

$\varepsilon_{Hf}(0) = ((^{176}Hf/^{177}Hf)_S/(^{176}Hf/^{177}Hf)_{CHUR}-1) \times 10000$; $\varepsilon_{Hf}(t) = ((^{176}Hf/^{177}Hf)_S - (^{176}Lu/^{177}Hf)_S \times (e^{\lambda t}-1))/((^{176}Hf/^{177}Hf)_{CHUR} - (^{176}Lu/^{177}Hf)_{CHUR} \times (e^{\lambda t}-1)-1) \times 10{,}000$; $T_{Hf1} = 1/\lambda \times \ln [1 + ((^{176}Hf/^{177}Hf)_S - (^{176}Hf/^{177}Hf)_{DM})/((^{176}Lu/^{177}Hf)_S - (^{176}Lu/^{177}Hf)_{DM})]$; $T_{Hf2} = T_{Hf1} - (T_{Hf1}-t)(f_{CC}-f_S)/(f_{CC}-f_{DM})$; $f_{Lu/Hf} = (^{176}Lu/^{177}Hf)_S/(^{176}Lu/^{177}Hf)_{CHUR}-1$ $(^{176}Lu/^{177}Hf)_{CHUR} = 0.0332$, $(^{176}Hf/^{177}Hf)_{CHUR} = 0.282772$ (Blichert-Toft and Albarède, 1997), $(^{176}Lu/^{177}Hf)_{DM} = 0.0384$, $(^{176}Hf/^{177}Hf)_{DM} = 0.2835$ (Griffin et al., 2000), $f_{CC} = [(^{176}Lu/^{177}Hf)_{mean\ crust}/(^{176}Lu/^{177}Hf)_{CHUR}] = 1$, $f_{DM} = [(^{176}Lu/^{177}Hf)_{DM}/(^{176}Lu/^{177}Hf)_{CHUR}] = 1$, $\lambda = 1.867 \times 10^{-11}$ year^{-1} (Söderlund et al., 2004), t = crystallization age of zircon. The 2σ represents standard deviation.

Table 6
Re–Os isotopic analytical data from the Mo-bearing Xiaoshuijing Syenogranite in the Tengchong Terrane.

Sample No.	Sample weight (g)	Re (ppm)		^{187}Re (ppm)		^{187}Os (ppb)		Model age (Ma)	
		Measured	2σ	Measured	2σ	Measured	2σ	Measured	2σ
HQ-18	0.00611	17.72	0.12	11.14	0.07	11.97	0.09	64.48	0.91
HQ-19	0.02031	14.44	0.14	9.076	0.085	9.797	0.096	64.76	1.09
HQ-20	0.02134	7.145	0.052	4.491	0.033	4.875	0.031	65.12	0.90
HQ-22	0.02079	6.612	0.046	4.156	0.029	4.588	0.035	66.23	0.95

Decay constant: $\lambda(^{187}Re) = 1.666 \times 10^{-11}$/year (Smoliar et al., 1996). Uncertainties are absolute at 2σ with error on Re and ^{187}Os concentrations and the uncertainty in the ^{187}Re decay constant.

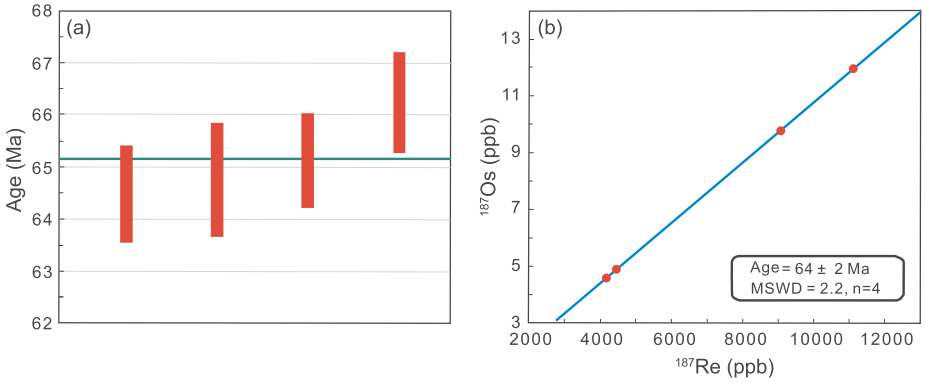

Fig. 8. Molybdenite Re-Os isochron and weighted mean model date for the Mo-mineralised Xiaoshuijing Syenogranite in the Tengchong Terrane.

5.2. Magma source

Ti-in-zircon thermometer is a tool with the potential to determine crystallisation temperatures of zircons (Watson and Harrison, 2005; Watson et al., 2006; Baldwin et al., 2007). The temperatures calculated by this method for the Xiaoshuijing Syenogranite are between 569° to 829 °C (Table 3; Dilles et al., 2015; Lee et al., 2017). The lowest temperature is at the amphibolite facies range and cannot be the temperature at which the syenogranite crystallised from a melt, therefore the upper value is here taken as being more plausible. This means that the syenogranite was emplaced at middle crustal levels of around 30 km, assuming a thermal gradient of 25–30 °C/km.

The high A/CNK values of 1.38–1.68 are indicative of aluminium enrichment during magmatic crystallisation. Aluminium enrichment would be the result of: (1) fractional crystallisation of amphibole and pyroxene, despite the source rocks not being saturated in Al (e.g. Chappell et al., 2012; Zen, 1986); (2) partial melting in the crust of basaltic to andesitic rocks (e.g. Ellis and Thompson, 1986); and (3) partial melting of Al-rich metasedimentary rocks (e.g. Nabelek and Glascock, 1995; Sylvester, 1998). Given that the Xiaoshuijing Syenogranite lacks hornblende and pyroxene and is petrographically an I-type granite, the first option is likely.

Hafnium (Hf) isotopic data obtained from zircons are often used in the study of crustal evolution (e.g. Belousova et al., 2002; Griffin et al., 2002a,b; Yang et al., 2007; Chiu et al., 2009; Ji et al., 2009; Xu et al., 2012; Qi et al., 2015). Positive $\varepsilon_{Hf}(t)$ values broadly indicate derivation from mantle-derived (juvenile) sources, and negative $\varepsilon_{Hf}(t)$ values indicate derivation, at least in part, from continental crust (e.g. Bahlburg et al., 2011). Using these criteria, samples of the Xiaoshuijing Syenogranite with negative $\varepsilon_{Hf}(t)$ values of −18.23 to −12.92 and T_{DM}^2 ages of 2281–1950 Ma are derived from a Paleoproterozoic igneous source in the middle to upper crust (Fig. 10).

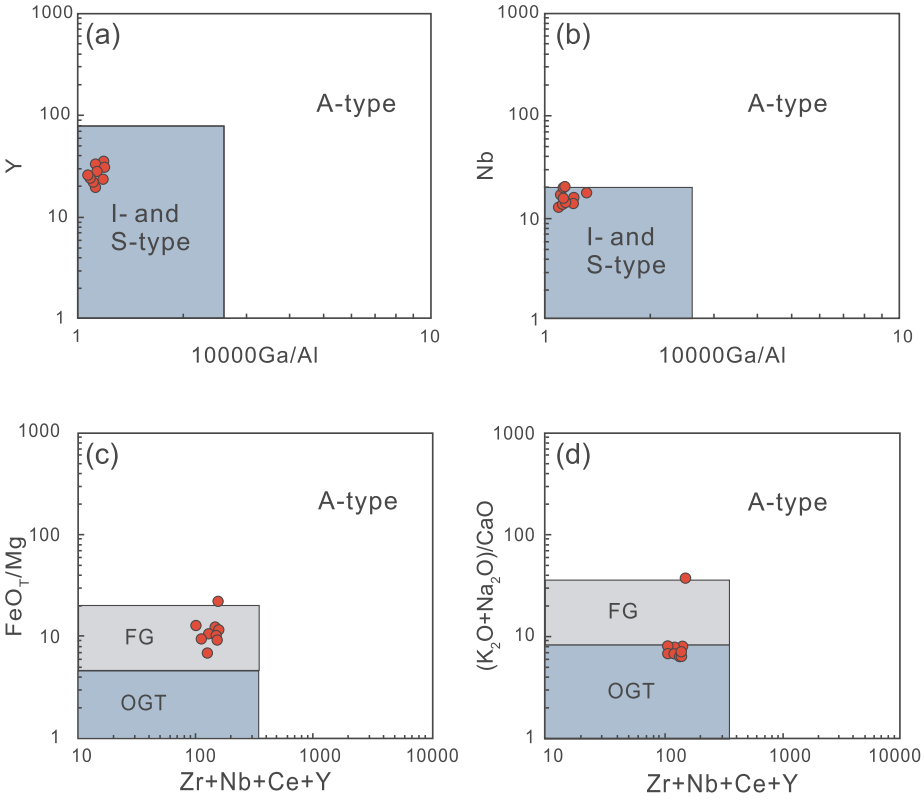

Fig. 9. Discrimination diagrams for the Mo-mineralised Xiaoshuijing Syenogranite in the Tengchong Terrane: (a) Y vs 10,000 × Ga/Al diagram (after Whalen et al., 1987); (b) Nb vs 10,000 × Ga/Al diagram (after Whalen et al., 1987); (c) FeO_T/MgO vs Zr + Nb + Ce + Y (after Whalen et al., 1987); (d) ($Na_2O + K_2O$)/CaO vs Zr + Nb + Ce + Y (after Whalen et al., 1987, all in molar proportion).

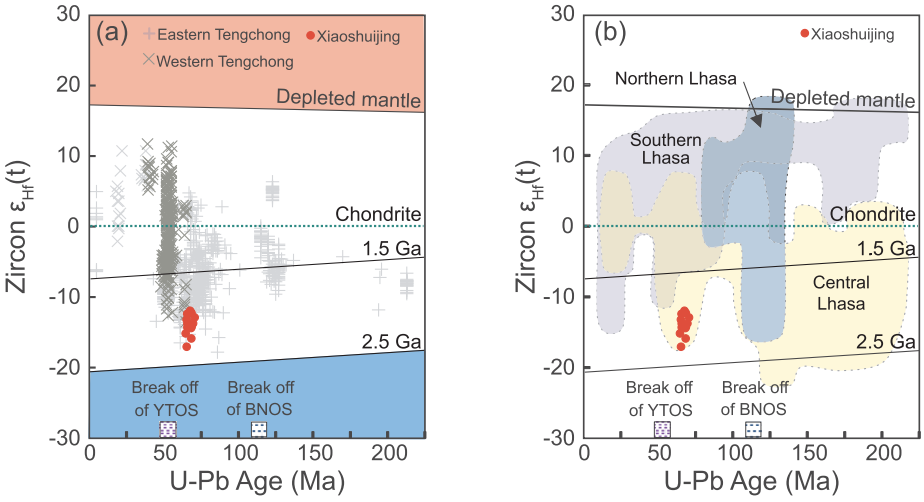

Fig. 10. Zircon $\varepsilon_{Hf}(t)$ vs U–Pb dates for the Mo-bearing Xiaoshuijing Syenogranite. For comparison, the fields of the Tengchong Terrane (a; after Cao et al., 2015) and Lhasa Block (b; after Hou et al., 2015) are outlined. The purple and black vertical bars represent the timing of the interpreted break-off of the subducted Tethyan Oceanic slabs at 113 ± 5 Ma for the Bangong–Nujiang Oceanic slab (BNOS) and at ca. 52 Ma for the Yarlung–Tsangpo Oceanic slab (YTOS) (after Hou et al., 2015). The calculated T_{DM}^2 model ages and notations of the Chondritic Uniform Reservoir (CHUR) and depleted mantle (DM) curves are given in the figure. (For interpretation of the references to colour in this figure legend, the reader is referred to the web version of this article.)

Additionally, the Hf-isotopic data of the Mesozoic to Cenozoic granites from the eastern and western parts of the Tengchong Terrane are indistinguishable from those of the granites in the Central and South Lhasa blocks (Fig. 10) (Qi et al., 2015; Xie et al., 2016; Cao et al., 2016). The Hf-isotopic data from the Xiaoshuijing Syenogranite in the eastern part of the Tengchong Terrane are like those of the Central Lhasa block (Fig. 7b). These similarities could mean that the two regions constitute a continuous and coincident arc-shaped magmatic and tectonic belt associated with the Late Cretaceous to Paleocene subduction of the Neo-Tethyan Ocean plate (Fig. 1a; Gardiner et al., 2015a, Xu et al., 2015b).

5.3. Mo mineralisation

The accuracy of Re-Os Mo dating has improved over the last fifteen years through new techniques, improved standards, and new equipment (Stein et al., 2003; Selby and Creaser, 2004; Xie et al., 2007; Li et al., 2010). Samples of disseminated Mo from the Xiaoshuijing Syenogranite yield a Re-Os age of 64 ± 2 Ma. The U-Pb zircon age of the syenogranite is dated at 65 ± 1 Ma, which is coeval with the Mo age within error. This is the first time that granite containing disseminated Mo mineralisation has been recognised in the Late Cretaceous to Early Cenozoic Binlang River granitic suite in the Tengchong Terrane (Fig. 11). Incidentally, disseminated Mo mineralisation has previously been recognised in the Early Cretaceous Xiaochang Granite in the NE part of the terrane (Chen et al., 2013).

The timing of the initial collision between the India with Eurasia plates is uncertain with numerous suggestions ranging from ca. 65 to 34 Ma (e.g. Jaeger et al., 1989; Klootwijk et al., 1992; Rowley, 1996; Mo et al., 2002, 2008; Leech et al., 2005; Yin, 2006; Aitchison et al., 2007; Yin and Harrison, 2000; Najman et al., 2010; Hu et al., 2012; Ma et al., 2014; Wang et al., 2014d). The Neo-Tethyan Ocean opened during the Triassic and closed following the Cretaceous to Paleogene

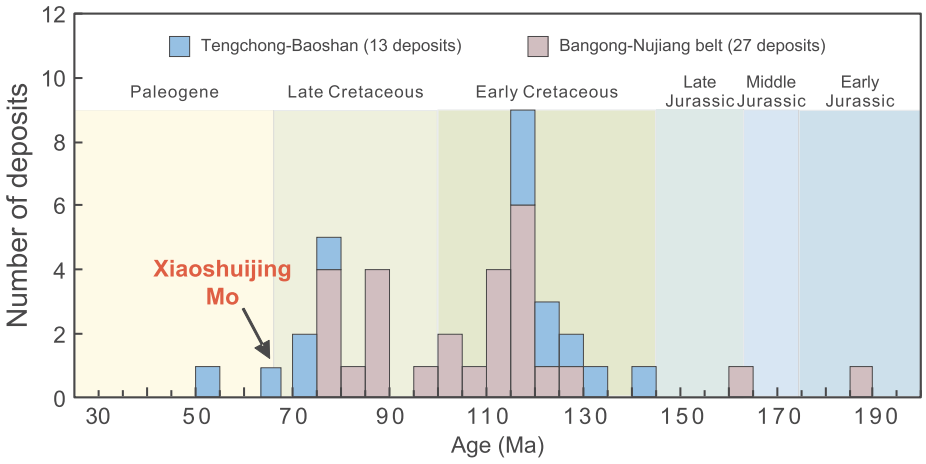

Fig.11. Histogram showing the number of deposits in the Bangong–Nujiang mineralised belt and the Tengchong–Baoshan area (Data sources and discussion from Cao et al., 2017a; Deng et al., 2014a; Ma et al., 2013; Hou et al., 2007).

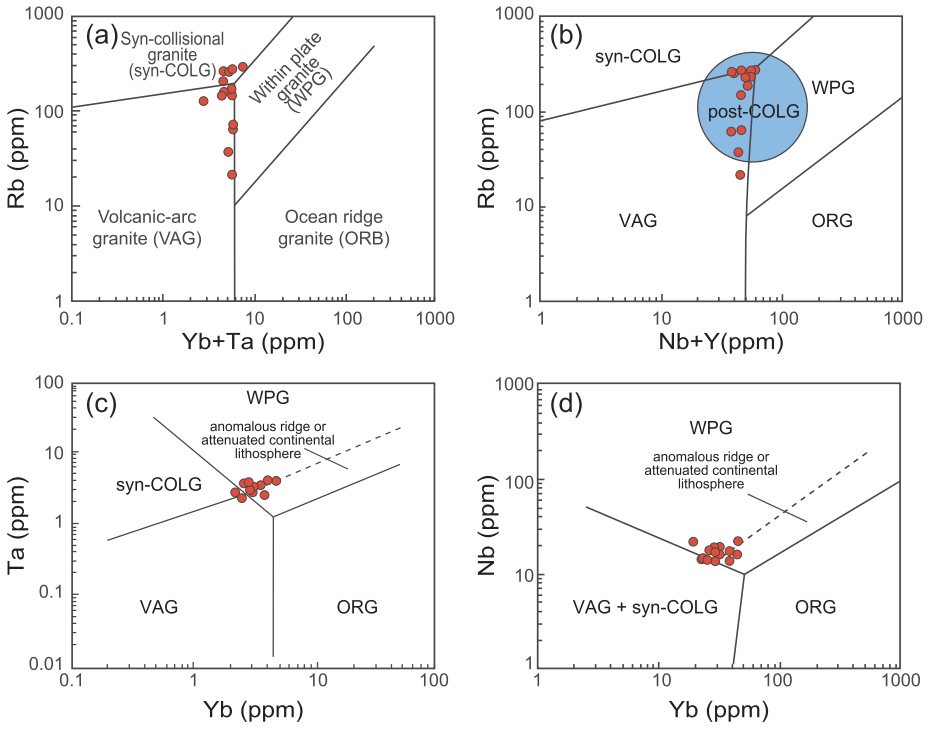

Fig. 12. Discrimination diagrams for the Xiaoshuijing Syenogranite: (a) Rb vs (Yb + Ta) plot; (b) Rb vs (Nb + Y) plot; (c) Ta vs Yb plot; and (d) Nb vs Yb plot (after Pearce, 1996). Abbreviations: Syn-COLG = syn-collisional granites; post-COLG = post-collisional granites; VAG = volcanic arc granites; ORG = ocean ridge granites; WPG = within-plate granites.

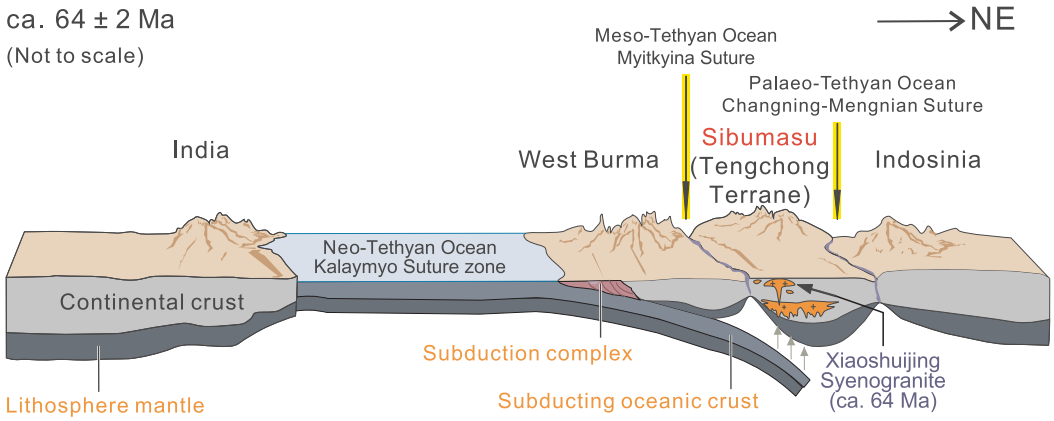

Fig.13. Schematic sketch displaying the tectonic settings for the generation of Early Paleogene magmatism and Mo-mineralisation in the western Yunnan district.

subduction of the Neo-Tethyan Ocean plate leading to the collision of the Indian and Eurasian continental plates (Mo et al., 1993; Zhong, 1998; Cong et al., 2009; Yang et al., 2009). It is envisaged that the Xiaoshuijing Syenogranite was emplaced during the subduction of the Neo-Tethyan Ocean plate at ca. 64 Ma. This was after its fractionation, the introduction of disseminated Mo probably sourced from the syenogranite's magma. Lerchbaumer and Audétat (2013) suggest that extraction of fractionated melts and their accumulation at the top of a magma chamber may be the most important requirement for the formation of economic deposits, such as at Xiaoshuijing.

It is proposed that the syenogranite represents a large volume fractionated, crystal-poor melt occupying shallow magma chambers, and the Mo content of the melt increased with fractionation given that Mo is immiscible (c.f. Zhang and Audétat, 2017). The magmatic–hydrothermal transition results from decreasing pressure and crystallisation as the magma approaches the surface. This process leads to the separation of immiscible phases, such as Mo, and their precipitation (Candela and Holland, 1986; Roedder, 1992; Beane and Bodnar, 1995). A quick rise of the magma towards the surface would result in the deposition of disseminated Mo in the fractionated syenogranite. A slower ascent to the surface would have allowed hydrothermal fluid to carry Mo in associated with quartz(–sulfide) veins with alteration envelopes containing minerals such as K-feldspar and sericite (Beane and Bodnar, 1995). On passing, the implication of this is that Late Cretaceous to Early Cenozoic (ca. 64 Ma) plutonic rocks are prospective for Mo. In addition to the ca. 120 and 80 Ma magmatic and mineralising events recognised in the Donghe and Guyong granitic suites (mentioned earlier) in the Tengchong Terrane, we now know that there was a ca. 64 Ma magmatic and Mo mineralising event in the Binlang River granitic suite in the terrane.

5.4. Tectonic setting

Using the discrimination diagrams of Harris et al. (1986) and Pearce (1996), the samples from the Xiaoshuijing Syenogranite plot in the within-plate and syn-collisional granites fields (Fig. 12). This can be interpreted to mean that the syenogranite was generated during subduction of the Neo-Tethyan Ocean plate during ca. 64 Ma before the collision of the Indian and Eurasian continents, as discussed above.

The Neo-Tethyan Ocean opened during the Middle Triassic and included many small oceanic basins separated by microcontinents and closed during the Early Cretaceous to Early Paleogene over a period of 90 million years (e.g. Stampfli, 2000). The Tengchong Terrane was intruded by granites before ca. 60 Ma in a subduction setting, ca. 59 Ma in a syn-collisional setting (e.g. Hu et al., 2015; Wang et al., 2014c), and after ca. 55 Ma in a post-collisional extensional event (e.g. Leech et al., 2005; Mo et al., 2007). On passing, it is interesting to note that the collision was diachronous starting at ca. 55 Ma in the Lhasa Terrane (Wang et al., 2014c). The Xiaoshuijing Syenogranite was emplaced during ca. 64 Ma in response to the subduction of the Neo-Tethyan Ocean plate, and melting of crustal thickening (Fig. 13; Zhao and Zhou, 2008; Zhu et al., 2009). The granites emplaced during this time are characterised by negative zircon $\varepsilon_{Hf}(t)$ values related to partial melting of the thickened crust (Zhao and Zhou, 2008; Zhu et al., 2009). The chondrite-normalised REE patterns of the syenogranite are indicative of a crustal origin, and the negative $\varepsilon_{Hf}(t)$ values of the syenogranite's zircons also suggest a crustal source.

The collision of continental plate, such as the collision of India with Eurasia, results in a significantly thickened crust reaching depths to the Moho of around 70–80 km (e.g. Koulakov et al., 2015). Similar thickness are documented for orogens in the North Australia Craton (Bagas et al., 2014). Recent tomographic studies indicate a crustal thickness variation along and across the Nepal Himalayas. The crustal thickness varies between 40 at the foothills of the Himalayas to 80 km at the high Himalayas, which is verified by synthetic modelling (Koulakov et al., 2015). Such a thickened crust is important in the genesis of mineralisation, such as Mo mineralisation, as shown by the presence of many deposits in Tibet.

The base of the ~80 km thickened lower crust in the Himalayas would reach temperatures of over 2000 °C, assuming a geothermal gradient of 30 °C/km (c.f. Thompson and Connolly, 1995; Clemens, 2003). An additional process that would elevate the temperature in the Tengchong Terrane includes the upwelling of the asthenosphere resulting from the subduction of the Neo-Tethyan Oceanic plate during the early stage of the India–Eurasian continental collision (e.g. Cao et al., 2017a; Zeng et al., 2017; Kohn and Parkinson, 2002). This process could also lead to the introduction of heated fluids from the subducted oceanic crust into the lower part of the crust in the Tengchong Terrane resulting in melting and emplacement of magma being the source of the Mo-bearing Xiaoshuijing Syenogranite.

6. Conclusions

Detailed geochemistry studies of the Mo-bearing Xiaoshuijing Syenogranite show that it is fractionated, enriched in Si, Al and K, depleted in Mg, Fe and Ca, and has an average aluminium saturation index (A/CNK) of 1.53. This is a high-K, alkaline and peraluminous syenogranite. The $\varepsilon_{Hf}(t)$ values for the zircon analysed from the syenogranite average −16.66, which is characteristic of a crustal source.

The Xiaoshuijing Syenogranite yields a U-Pb zircon date of 65 ± 1 Ma and the disseminated Mo mineralisation in the syenogranite yield an Early Paleogene Re-Os age of 64 ± 2 Ma. These dates show that the syenogranite and Mo are coeval having the same age within error.

Ti-in-zircon temperature ($T_{Ti\text{-}in\text{-}zirc}$) of the Xiaoshuijing Syenogranite varies widely from 569° to 829 °C, which theoretically represents the approximate crystallisation temperature of the magma. The lower temperature limit of 569 °C, characteristic of the lower amphibolite facies, is considered too low to be valid and the temperature at the higher end of the range seems more plausible. The syenogranite is a syn-collisional, peraluminous granite related to the closure of Neo-Tethys Ocean. This was during the subduction of the Neo-Tethys Ocean plate before the collision of the India and Eurasian continental plates that resulted in crustal thickening.

The tectonic events during the emplacement of the Xiaoshuijing Syenogranite include subduction, and the generation of magma associated with Mo mineralisation. This marks a significant period of magmatism and mineralisation increasing the prospectivity of the Tengchong Terrane in SW China.

Acknowledgements

We are grateful to the three anonymous reviewers, Editor-in-Chief Prof. Franco Pirajno, Associate Editor Dr Yanbo Cheng, Prof. Zhanzhang Xu, Dr Li Tang, and Dr Yi Fang for their helpful comments improving this contribution. This study is financially supported by the National Natural Science Foundation of China (41702108 and 41802095), China Scholarship Council (201608515058) and Major cultivating project of Sichuan Province Education Department (2018CZ0009).

References

Aitchison, J.C., Ali, J.R., Davis, A.M., 2007. When and where did India and Asia collide? J. Geophys. Res.-Solid Earth 112, B05423.

Amelin, Y., Lee, D.C., Halliday, A.N., 2000. Early-middle Archaean crustal evolution deduced from Lu-Hf and U-Pb isotopic studies of single zircon grains. Geochim. Cosmochim. Acta 64, 4205–4225.

Andersen, T., 2002. Correction of common lead in U-Pb analyses that do not report ^{204}Pb. Chem. Geol. 192, 59–79.

Bagas, L., Boucher, R., Li, B., Miller, J., Hill, P., Depauw, G., Pascoe, J., Eggers, B., 2014. Paleoproterozoic stratigraphy and gold mineralisation in the Granites-Tanami Orogen, North Australian Craton. Aust. J. Earth Sci. 61, 89–111.

Bahlburg, H., Vervoot, J.D., Dufrane, S.A., Carlotto, V., Reimann, C., Cárdenas, J., 2011. The U-Pb and Hf isotope evidence of detrital zircons of the Ordovician Ollantaytambo

Formation, southern Peru, and the Ordovician provenance and paleogeography of southern Peru and northern Bolivia. J. Sth Am. Earth Sci. 32 (3), 196–209.
Baldwin, J.A., Brown, M., Schmitz, M.D., 2007. First application of titanium-in-zircon thermometry to ultrahigh-temperature metamorphism. Geology 35, 295–298.
Beane, R.E., Bodnar, R.J., 1995. Hydrothermal fluids and hydrothermal alteration in porphyry copper deposits. In: Pierce, F.W., Bohm, J.G. (Eds.), Porphyry copper deposits of American Cordillera. Arizona Geological Society Digest, pp. 83–93 vol. 20.
Belousova, E.A., Griffin, W.L., O'Reilly, S.Y., Fisher, N.I., 2002. Igneous zircon: trace element composition as an indicator of source rock type. Contrib. Mineral Petrol. 143, 602–622.
Blichert-Toft, J., Albarède, F., 1997. The Lu-Hf isotope geochemistry of chondrites and the evolution of the mantle-crust system. Earth Planet Sci. Lett. 148, 243–258.
Candela, P.A., Holland, H.D., 1986. A mass transfer model for copper and molybdenum in magmatic-hydrothermal systems: the origin of porphyry-type ore deposits. Econ. Geol. 81, 1–19.
Cao, H.W., Zhang, S.T., Lin, J.Z., Zheng, L., Wu, J.D., Li, D., 2014. Geology, geochemistry and geochronology of the Jiaojiguanliangzi Fe-polymetallic deposit, Tengchong County, Western Yunnan (China): regional tectonic implications. J. Asian Earth Sci. 81, 142–152.
Cao, H.W., Zhang, S.T., Santosh, M., Zheng, L., Tang, L., Li, D., Zhang, X.H., Zhang, Y.H., 2015. The Luanchuan Mo–W–Pb–Zn–Ag magmatic–hydrothermal system in the East Qinling metallogenic belt, China: constrains on metallogenesis from C-H–O–S–Pb isotope compositions and Rb–Sr isochron ages. J. Asian Earth Sci. 111, 751–780.
Cao, H.W., Zou, H., Zhang, Y.H., Zhang, S.T., Zheng, L., Zhang, L.K., Pei, Q.M., 2016. Late Cretaceous magmatism and related metallogeny in the Tengchong area: evidence from geochronological, isotopic and geochemical data from the Xiaolonghe Sn deposit, western Yunnan. China. Ore Geol. Rev. 78, 196–212.
Cao, H.W., Zhang, Y.H., Santosh, M., Zhang, S.T., Tang, L., Pei, Q.M., Yang, Q.Y., 2017b. Mineralogy, zircon U-Pb-Hf isotopes, and whole-rock geochemistry of Late Cretaceous-Eocene granites from the Tengchong terrane, western Yunnan, China: record of the closure of the Neo-Tethyan Ocean. Geol. J. https://doi.org/10.1002/gj.2964.
Cao, H.W., Zhang, Y.H., Pei, Q.M., Zhang, R.Q., Tang, L., Lin, B., Cai, G.J., 2017a. U-Pb dating of zircon and cassiterite from the Early Cretaceous Jiaojiguan iron-tin polymetallic deposit, implications for magmatism and metallogeny of the Tengchong area, western Yunnan. China. Int. Geol. Rev. 59, 234–258.
Chappell, B.W., Bryant, C.J., Wyborn, D., 2012. Peraluminous I-type granites. Lithos 153, 142–153.
Chappell, B.W., White, A.J.R., 1974. Two contrasting granite types. Pac. Geol. 8, 173–174.
Chappell, B.W., White, A.J.R., 1992. I- and S-type granites in the Lachlan fold belt. Geol. Soc. of Am. Special Papers 272, 1–26.
Chen, J.C., 1987. Discussion on the age division and the selects of isotopic age determination for granitic rock in Western Yunnan. Yunnan Geol. 6, 101–113 (in Chinese with English abstract).
Chen, X.C., Hu, R.Z., Bi, X.W., Zhong, H., Lan, J.B., Zhao, C.H., Zhu, J.J., 2015. Petrogenesis of metaluminous A-type granitoids in the Tengchong-Lianghe tin belt of southwestern China: evidences from zircon U-Pb ages and Hf–O isotopes, and whole-rocks Sr–Nd isotopes. Lithos 212–215, 93–110.
Chen, F.K., Li, Q.L., Wang, X.L., Li, X.H., 2005. Early Paleozoic magmatism in Baoshan-Tengchong Block of the Tethyan Belt, Yunnan Province. Acta Geosci. Sin. 26, 93 (in Chinese with English abstract).
Chen, X.C., Hu, R.Z., Bi, X.W., Li, H.M., Lan, J.B., Zhao, C.H., Zhu, J.J., 2014. Cassiterite LA-MCICP-MS U-Pb and muscovite 40Ar/39Ar dating of tin deposits in the Tengchong-Lianghe tin district, NW Yunnan, China. Mineral. Deposita 49, 843–860.
Chen, F.K., Li, X.H., Wang, X.L., Li, Q.L., Siebel, W., 2007. Zircon age and Nd–Hf isotopic composition of the Yunnan Tethyan belt, southwestern China. Int. J. Earth Sci. 96, 1179–1194.
Chen, J.S., Lin, W.X., Chen, L.Z., 1991. Series and unit research on Tin-bearing granites of Tengchong-Lianghe area. Yunnan Geol. 10, 241–289 (in Chinese with English abstract).
Chen, Y.Q., Lu, Y.X., Zhao, H.J., Cheng, Z.Z., Jiang, C.X., Liu, Z.S., 2013. Zircon SHRIMP U-Pb geochronology, geochemistry of the Xiaochang monzonitic granite with Mo mineralization and implications for tectonic setting in Tengchong Block, Western Yunnan terrain, Southwestern China. Earth Sci. Front. 20, 1–14.
Chen, B., Xie, G., 1994. Evolution of the Tethys in Yunnan and Tibet. J. SE Asian Earth Sci. 9, 349–354.
Chiu, H.Y., Chung, S.L., Wu, F.Y., Liu, D., Liang, Y.H., Lin, I.J., Iizuka, Y., Xie, L.W., Wang, Y., Chu, M.F., 2009. Zircon U-Pb and Hf isotopic constraints from eastern Transhimalayan batholiths on the precollisional magmatic and tectonic evolution in southern Tibet. Tectonophysics 477, 3–19.
Clairborne, L.L., Miller, C.F., Walker, B.A., Wooden, J.L., Mazdab, F.K., Bea, F., 2006. Tracking magmatic processes through Zr/Hf ratios in rocks and Hf and Ti zoning in zircons: an example from the Spirit Mountain batholith, Nevada. Mineral Mag. 70, 517–543.
Clemens, J.D., 2003. S-type granitic magmas—petrogenetic issues, models and evidence. Earth-Sci. Rev. 61, 1–18.
Collins, W.J., Beams, S.D., White, A.J.R., Chappell, B.W., 1982. Nature and origin of A-type granites with particular reference to southeastern Australia. Contrib. Mineral. Petrol. 80, 189–200.
Cong, F., Lin, S.L., Li, Z.H., Zou, G.F., Geng, Q.R., 2009. Zircon U-Pb age of Gneissic Granites in the Tengchong Block, Western Yunnan. Acta Geol. Sin. 83, 651–658 (in Chinese with English abstract).
Cong, F., Lin, S.L., Zou, G.F., Li, Z.H., Xie, T., Peng, Z.M., Liang, T., 2011. Magma mixing of granites at Lianghe: in-situ zircon analysis for trace elements, U-Pb ages and Hf isotopes. Sci. China Earth Sci. 54, 1346–1359.
Deng, J., Wang, Q.F., Li, G.J., Li, C.S., Wang, C.M., 2014a. Tethys tectonic evolution and its bearing on the distribution of important mineral deposits in the Sanjiang region, SW China. Gondwana Res. 26, 419–437.
Deng, J., Wang, Q.F., Li, G.J., Santosh, M., 2014b. Cenozoic tectono-magmatic and metallogenic processes in the Sanjiang region, southwestern China. Earth-Sci. Rev. 138, 268–299.
Dilles, J.H., Kent, A.J.R., Wooden, J.L., Tosdal, R.M., Koleszar, A., Lee, R.G., Farmer, L.P., 2015. Zircon compositional evidence for sulfur-degassing from ore-forming arc magmas. Econ Geol. 110, 241–251.
Dong, M.L., Dong, G.C., Mo, X.X., Santosh, M., Zhu, D.C., Yu, J.C., Nie, F., Hu, Z.C., 2013. Geochemistry, zircon U-Pb geochronology and Hf isotopes of granites in the Baoshan Block, Western Yunnan: implications for Early Paleozoic evolution along the Gondwana margin. Lithos 179, 36–47.
Dong, F.L., Hou, Z.Q., Gao, Y.F., Jiang, C.X., Du, A.D., 2005. Re-Os isotopic dating of molybdenite from Datongchang copper-lead-zinc deposit in Tengchong area, western Yunnan. Miner. Depos. 24, 663–668 (in Chinese with English abstract).
Dong, F.L., Hou, Z.Q., Gao, Y.F., Zeng, P.S., Jiang, C.X., 2006. Cenozoic granitoid in Tengchong, western Yunnan: genesis type and implication of tectonics. Acta Petrol. Sin. 22, 927–937 (in Chinese with English abstract).
Ellis, D.J., Thompson, A.B., 1986. Subsolidus and partial melting reactions in the quartz-excess $CaO+MgO+Al_2O_3+SiO_2+H_2O$ system under water-excess and water-deficient conditions to 10 kb: some implications for the origin of peraluminous melts from mafic rocks. J. Petrol. 27, 91–121.
Ferry, J.M., Watson, E.B., 2007. New thermodynamic models and revised calibrations for the Ti-in-zircon and Zr-in-rutile thermometers. Contrib. Mineral. Petrol. 154, 429–437.
Gao, J.F., Zhou, M.F., Robinson, P.T., Wang, C.Y., Zhao, J.H., Malpas, J., 2015. Magma mixing recorded by Sr isotopes of plagioclase from dacites of the Quaternary Tengchong volcanic field, SE Tibetan Plateau. J. Asian Earth Sci. 98, 1–17.
Geng, J.Z., Li, H.K., Zhang, J., Zhou, H.Y., Li, H.M., 2011. Zircon Hf isotope analysis by means of LA-MC-ICP-MS. Geol. Bul. China 30, 1508–1513 (in Chinese with English abstract).
Griffin, W.L., Pearson, N.J., Belousova, E., Jackson, S.E., van Achterbergh, E., O'Reilly, S.Y., Shee, S.R., 2000. The Hf isotope composition of cratonic mantle: LAM-MCICPMS analysis of zircon megacrysts in kimberlites. Geochim. Cosmochim. Acta 64, 133–147.
Griffin, W.L., Wang, X., Jackson, S.E., Pearson, N.J., O'Reilly, S.Y., Xu, X., Zhou, X., 2002b. Zircon chemistry and magma genesis, SE China: in-situ analysis of Hf isotopes, Tonglu and Pingtan Igneous complexes. Lithos 61 (3–4), 237–269.
Griffin, W.L., Belousova, E.A., Shee, S.R., Pearson, N.J., O'Reilly, S.Y., 2002a. Archean crustal evolution in the northern Yilgarn Craton: U-Pb and Hf-isotope evidence from detrital zircons. Precambrian Res. 131, 231–282.
Grimes, C.B., Wooden, J.L., Cheadle, M.J., John, B.E., 2015. "Fingerprinting" tectono-magmatic provenance using trace elements in igneous zircon. Contrib. Mineral. Petrol. 170, 1–26.
Harris, N.B., Pearce, J.A., Tindle, A.G., 1986. Geochemical characteristics of collision-zone magmatism. Geol. Soc., London, Special Publications 19 (1), 67–81.
Hoskin, P.W., 2005. Trace-element composition of hydrothermal zircon and the alteration of Hadean zircon from the Jack Hills, Australia. Geochim. Cosmochim. Acta 69, 637–648.
Hoskin, P.W.O., Schaltegger, U., 2003. The composition of zircon and igneous and metamorphic petrogenesis. Rev. Mineral. Geochem. 53, 27–62.
Hou, Z.Q., Zaw, K., Pan, G.T., Mo, X.X., Xu, Q., Hu, Y.Z., Li, X.Z., 2007. Sanjiang Tethyan metallogenesis in S.W. China: tectonic setting, metallogenic epochs and deposit types. Ore Geol. Rev. 31, 48–87.
Hou, Z.Q., Yang, Z.M., Lu, Y.J., Kemp, A., Zheng, Y.C., Li, Q.Y., Tang, J.X., Yang, Z.S., Duan, L.F., 2015. A genetic linkage between subduction- and collision-related porphyry Cu deposits in continental collision zones. Geology 43, 247–250.
Hu, X., Sinclair, H.D., Wang, J., Jiang, H., Wu, F., 2012. Late Cretaceous-Palaeogene stratigraphic and basin evolution in the Zhepure Mountain of southern Tibet: implications for the timing of India-Asia initial collision. Basin Res. 24, 520–543.
Hu, X., Garzanti, E., Moore, T., Raffi, I., 2015. Direct stratigraphic dating of India-Asia collision onset at the Selandian (middle Paleocene, 59 ± 1 Ma). Geology 43, 859–862.
Jaeger, J.J., Courtillot, V., Tapponnier, P., 1989. Paleontological view of the ages of the Deccan Traps, the Cretaceous/Tertiary boundary, and the India-Asia collision. Geology 17, 316–319.
Ji, W.Q., Wu, F.Y., Chung, S.L., Li, J.X., Liu, C.Z., 2009. Zircon U-Pb geochronology and Hf isotopic constraints on petrogenesis of the Gangdese batholith, southern Tibet. Chem. Geol. 262, 229–245.
Jiang, B., Gong, Q.J., Zhang, J., Ma, N., 2012. Late Cretaceous aluminium A-type granites and its geological significance of Dasongpo Sn deposit, Tengchong, West Yunnan. Acta Petrol. Sin. 28, 1477–1492 (in Chinese with English abstract).
Klootwijk, C.T., Gee, J.S., Peirce, J.W., Smith, G.M., McFadden, P.L., 1992. An early India-Asia contact: paleomagnetic constraints from Ninetyeast Ridge, ODP Leg 121. Geology 20 (5), 395–398.
Kohn, M.J., Parkinson, C.D., 2002. Petrologic case for Eocene slab break off during the Indo-Asian collision. Geology 30, 591–594.
Koulakov, I., Maksotova, G., Mukhopadhyay, S., Raoof, J., Kaya, J.R., Jakovlev, A., Vasilevsky, A., 2015. Variations of the crustal thickness in Nepal Himalayas based on tomographic inversion of regional earthquake data. Solid Earth 6, 207–216.
Lee, R.G., Dilles, J.H., Tosdal, R.M., Wooden, J.L., Mazdab, F.K., 2017. Magmatic evolution of granodiorite intrusions at the El Salvador porphyry copper deposit, Chile, based on trace element composition and U/Pb age of zircons. Econ. Geol. 112, 245–273.
Lee, C.T.A., Morton, D.M., 2015. High silica granites: terminal porosity and crystal

settling in shallow magma chambers. Earth Planet. Sci. Lett. 409, 23–31.
Leech, M.L., Singh, S., Jain, A.K., Klemperer, S.L., Manickavasagam, R.M., 2005. The onset of India-Asia continental collision: early, steep subduction required by the timing of UHP metamorphism in the western Himalaya. Earth Planet. Sci. Lett. 234, 83–97.
Lerchbaumer, L., Audétat, A., 2013. The metal content of silicate melts and aqueous fluids in subeconomically Mo mineralized granites: implications for porphyry Mo genesis. Econ. Geol. 108, 987–1013.
Li, D.P., Luo, Z.H., Chen, Y.L., Liu, J.Q., Jin, Y., 2014. Deciphering the origin of the Tengchong block, west Yunnan: evidence from detrital zircon U-Pb ages and Hf isotopes of Carboniferous strata. Tectonophysics 614, 66–77.
Li, J.W., Deng, X.D., Zhou, M.F., Liu, Y.S., Zhao, X.F., Guo, J.L., 2010. Laser ablation ICP-MS titanite U-Th-Pb dating of hydrothermal ore deposits: a case study of the Tonglushan Cu-Fe-Au skarn deposit, SE Hubei Province, China. Chem. Geol. 270, 56–67.
Li, Y.L., He, H.Y., Wang, C.S., Wei, Y.S., Chen, X., He, J., Ning, Z.J., Zhou, A., 2017b. Early Cretaceous (ca. 100 Ma) magmatism in the southern Qiangtang subterrane, central Tibet: product of slab break-off? Int. J. Earth Sci. 106, 1289–1310.
Li, G.M., Qin, K.Z., Li, J.X., Evans, N.J., Zhao, J.X., Cao, M.J., Zhang, X.N., 2017a. Cretaceous magmatism and metallogeny in the Bangong-Nujiang metallogenic belt, central Tibet: evidence from petrogeochemistry, zircon U-Pb ages, and Hf-O isotopic compositions. Gondwana Res. 41, 110–127.
Liu, S., Hu, R.Z., Gao, S., Feng, C.X., Huang, Z.L., Lai, S.C., Yuan, H.L., Liu, X.M., Coulson, I.M., Feng, G.Y., Wang, T., Qi, Y.Q., 2009. U-Pb zircon, geochemical and Sr-Nd-Hf isotopic constraints on the age and origin of Early Palaeozoic I-type granite from the Tengchong-Baoshan Block, Western Yunnan Province, SW China. J. Asian Earth Sci. 36, 168–182.
Liu, Y., Hu, Z., Zong, K., Gao, C., Gao, S., Xu, J., Chen, H., 2010. Reappraisal and refinement of zircon U-Pb isotope and trace element analyses by LA-ICP-MS. Chin. Sci. Bull. 55, 1535–1546.
Liu, Z.Q., Li, X.Z., Ye, Q.T., 1993. Division of Tectono-magmatic Zones and the Distribution of Deposits in the Sanjiang Area. Geological Publishing House, Beijing, pp. 246 (in Chinese).
Lu, B.X., Wang, Z., Zhang, N.D., 1993. Granitoids and Metallogenetic Specialization of the Sanjiang Area. Geological Publishing House, Beijing, pp. 328 (in Chinese).
Ludwig, K.R., 2012. User's Manual for Isoplot 3.75: A Geochronological Toolkit for Microsoft Excel. Berkeley Geochronology Center, pp. 70.
Luo, J.L., 1990. Evolution of the basic characteristics of the Tethys orogenic zone, Western Yunnan. Yunnan Geol. 9, 247–290.
Ma, N., Deng, J., Wang, Q.F., Wang, C.M., Zhang, J., Li, G.J., 2013. Geochronology of the Dasongpo tin deposit, Yunnan Province: evidence from zircon LA-ICP-MS U-Pb ages and cassiterite LA-MC-ICP-MS U-Pb age. Acta Petrol. Sin. 29, 1223–1235 (in Chinese with English abstract).
Ma, L.Y., Wang, Y.J., Fan, W.M., Geng, H.Y., Cai, Y.F., Zhong, H., Liu, H.C., Xing, X.W., 2014. Petrogenesis of the early Eocene I-type granites in west Yingjiang (SW Yunnan) and its implication for the eastern extension of the Gangdese batholiths. Gondwana Res. 25, 401–419.
Maniar, P.D., Piccoli, P.M., 1989. Tectonic discrimination of granitoids. Geol. Soc. Am. Bull. 101, 635–643.
McDonough, W.F., Sun, S.S., 1995. The composition of the Earth. Chem. Geol. 120, 223–253.
Mo, X.X., Lu, F.X., Shen, S.Y., Zhu, Q.W., Hou, Z.Q., 1993. Volcanism and Metallogeny in the Sanjiang Tethys. Geological Publishing House, Beijing, pp. 178–235 (in Chinese).
Mo, X.X., Zhao, Z.D., Zhou, S., Dong, G.C., Guo, T., Wang, L., 2002. Evidence for Timing of the Initiation of India-Asia Collision from Igneous Rocks in Tibet. American Geophysical Union, Fall Meeting 2002, Abstract S62B-1201.
Mo, X.X., Hou, Z.Q., Niu, Y.L., Dong, G.C., Qu, X.M., Zhao, Z.D., Yang, Z.M., 2007. Mantle contributions to crustal thickening during continental collision: evidence from Cenozoic igneous rocks in southern Tibet. Lithos 96, 225–242.
Mo, X.X., Niu, Y.L., Dong, G.C., Zhao, Z.D., Hou, Z.Q., Zhou, S., Ke, S., 2008. Contribution of syncollisional felsic magmatism to continental crust growth: a case study of the Paleogene Linzizong volcanic succession in southern Tibet. Chem. Geol. 250, 49–67.
Morel, M.L.A., Nebel, O., Nebel-Jacobsen, Y.J., Miller, J.B., Vroon, P.Z., 2008. Hafnium isotope characterization of the GJ-1 zircon reference material by solution and laser-ablation MC-ICPMB. Chem. Geol. 255, 231–235.
Nabelek, P.I., Glascock, M.D., 1995. REE-depleted leucogranites, Black Hills, South Dakota: a consequence of disequilibrium melting of monazite-bearing schists. J. Petrol. 36 (4), 1055–1071.
Najman, Y., Appel, E., Boudagher-Fadel, M., Bown, P., Carter, A., Garzanti, E., Godin, L., Han, J., Liebke, U., Oliver, G., 2010. Timing of India-Asia collision: geological, biostratigraphic, and palaeomagnetic constraints. J. Geophys. Res. 115, B12416. https://doi.org/10.1029/2010JB007673.
NRGST, No. 6 Regional Geological Surveying Team, 1985. Geology Report on Regional Surveys of the 1:50,000 Tengchong and Langpuzhai Sheet. Yunnan Bureau of Geology and Mineral Exploration and Development, Kunming, 300 p (in Chinese).
Pan, G.T., Zhu, D.C., Wang, L.Q., Liao, Z.L., Geng, Q.R., Jiang, X.S., 2004. Bangong lake-Nujiang River suture zone-the northern boundary of Gondwana: evidence from geology and geophysics. Earth Sci. Front. 11, 371–382.
Pearce, J.A., 1996. Sources and settings of granitic rocks. Episodes 4, 120–125.
Pirajno, F., 2013. The Geology and Tectonic Settings of China's Mineral Deposits. Springe, Dordrecht.
Qi, X.X., Zhu, L.H., Grimmer, J.C., Hu, Z.C., 2015. Tracing the Transhimalayan magmatic belt and the Lhasa block southward using zircon U-Pb, Lu-Hf isotopic and geochemical data: Cretaceous-Cenozoic granitoids in the Tengchong block, Yunnan, China. J. Asian Earth Sci. 110, 170–188.
Roedder, E., 1992. Fluid inclusion evidence for immiscibility in magmatic differentiation. Geochim. Cosmochim. Acta 56 (1), 5–20.
Rowley, D.B., 1996. Age of initiation of collision between India and Asia: a review of stratigraphic data. Earth Planet. Sci. Lett. 145, 1–3.
Rubatto, D., 2002. Zircon trace element geochemistry: partitioning with garnet and the link between U-Pb ages and metamorphism. Chem. Geol. 184, 123–138.
Rudnick, R.L., Fountain, D.M., 1995. Nature and composition of the continental crust: a lower crustal perspective. Rev. Geophys. 33, 267–309.
Selby, D., Creaser, R.A., 2004. Macroscale NTIMS and microscale LA-MC-ICP-MS Re-Os isotopic analysis of molybdenite: testing spatial restrictions for reliable Re-Os age determinations, and implications for the decoupling of Re and Os within molybdenite. Geochim. Cosmochim. Acta 68, 3897–3908.
Shi, L., Chen, J.C., Wu, S.L., Peng, X.J., Tang, S.C., 1989. Metallogenic Regularity of Western Yunnan Sn Belt. Geological Publishing House, Beijing, pp. 200 (in Chinese).
Smoliar, M.I., Walker, R.J., Morgan, J.W., 1996. Re-Os ages of group IIA, IIIA, IVA, and IVB iron meteorites. Science 271 (5252), 1099–1102.
Söderlund, U., Patchett, P.J., Vervoort, J.D., Isachsen, C.E., 2004. The ^{176}Lu decay constant determined by Lu-Hf and U-Pb isotope systematics of Precambrian mafic intrusions. Earth Planet Sci. Lett. 219, 311–324.
Stampfli, G.M., 2000. Tethyan oceans. Special Publications 173 In: Bozkurt, E., Winchester, J.A., Piper, J.D.A. (Eds.), Tectonics and Magmatism in Turkey and the Surrounding Area. Geological Society, London, pp. 1–23.
Stein, H., Scherstén, A., Hannah, J., Markey, R., 2003. Subgrain-scale decoupling of Re and 187 Os and assessment of laser ablation ICP-MS spot dating in molybdenite. Geochim. Cosmochim. Acta 67, 3673–3686.
Sun, S.S., McDonough, W.F., 1989. Chemical and isotopic systematics of oceanic basalts: implications for mantle composition and processes. Geol. Soc. Lond., Spec. Publ. 42, 313–345.
Sylvester, P.L., 1998. Post-collisional strongly peraluminous granites. Lithos 45, 29–44.
Tao, Y., Zhu, F.L., Ma, Y.S., Ye, L., Chen, Z.T., 2009. LA-ICP-MS zircon U-Pb analysis of Zhibenshan granite, Baoshan Terrane. Acta Mineral. Sin. S1329 (supp.) (in Chinese).
Tao, Y., Hu, R.Z., Zhu, F.L., Ma, Y.S., Ye, L., Cheng, Z.T., 2010. Ore-forming age and the geodynamic background of the Hetaoping lead-zinc deposit in Baoshan, Yunnan. Acta Petrol. Sin. 26, 1760–1772 (in Chinese with English abstract).
Thompson, A.B., Connolly, A.D., 1995. Melting of the continental crust: some thermal and petrological constraints on anatexis in continental collision zones and other tectonic settings. J. Geophys. Res. 100, 15565–15579.
Trail, D., Watson, E.B., Tailby, N.D., 2012. Ce and Eu anomalies in zircon as proxies for the oxidation state of magmas. Geochim. Cosmochim. Acta 97, 70–87.
Wang, Y.J., Fan, W.M., Zhang, Y.H., Peng, T.P., Chen, X.Y., Xu, Y.G., 2006. Kinematics and 40Ar/39Ar geochronology of the Gaoligong and Chongshan shear systems, western Yunnan, China: implications for early Oligocene tectonic extrusion of SE Asia. Tectonophysics 418, 235–254.
Wang, G., Wan, J.L., Wang, E., Zheng, D.W., Li, F., 2008. Late Cenozoic to recent transtensional deformation across the southern part of the Gaoligong shear zone between the Indian plate and SE margin of the Tibetan plateau and its tectonic origin. Tectonophysics 460, 1–20.
Wang, C.M., Deng, J., Carranza, J.M.E., Santosh, M., 2014d. Tin metallogenesis associated with granitoids in the southwestern Sanjiang Tethyan Domain: nature, deposit types, and tectonic setting. Gondwana Res. 26 (2), 576–593.
Wang, G.Q., Liu, Z.H., Gao, X.L., Wu, J., Huang, W.T., Zou, Y.Q., Lin, S.P., Liang, H.Y., 2014b. Zircon LA-ICP_MS U-Pb age and molybdenite Re-Os dating of the Maliba molybdenum- copper-lead-zinc deposit and its geological significance in the Tengchong area, Western Yunnan. Acta Geol. Sin. 88, 2097–2107.
Wang, F., Liu, F., Liu, P., Shi, J., Cai, J., 2014a. Petrogenesis of Lincang granites in the south of Lancangjiang area: constrain from geochemistry and zircon U-Pb geochronology. Acta Petrol. Sin. 30, 3034–3050 (in Chinese with English abstract).
Wang, Y.J., Xing, X.W., Cawood, P.A., Lai, S.C., Xia, X.P., Fan, W.M., Liu, H.C., Zhang, F.F., 2013. Petrogenesis of early Paleozoic peraluminous granite in the Sibumasu Block of SW Yunnan and diachronous accretionary orogenesis along the northern margin of Gondwana. Lithos 182–183, 67–85.
Wang, Y.J., Zhang, L., Cawood, P.A., Ma, L., Fan, W., Zhang, A., Bi, X., 2014c. Eocene supra-subduction zone mafic magmatism in the Sibumasu Block of SW Yunnan: implications for Neotethyan subduction and India-Asia collision. Lithos 206, 384–399.
Watson, E.B., Harrison, T.M., 2005. Zircon thermometer reveals minimum melting conditions on earliest Earth. Science 308, 841–844.
Watson, E., Wark, D., Thomas, J., 2006. Crystallization thermometers for zircon and rutile. Contrib. Mineral. Petrol. 151 (4), 413–433.
Whalen, J.B., Currie, K.L., Chappell, B.W., 1987. A-type granites: geochemical characteristics, discrimination and petrogenesis. Contrib. Mineral. Petrol. 95, 407–419.
Whitehouse, M.J., Platt, J.P., 2003. Dating high-grade metamorphism constraints from rare earth elements in zircon and garnet. Contrib. Mineral. Petrol. 145, 61–74.
Wright, J.B., 1969. A simple alkalinity ratio and its application to questions of non-orogenic granite genesis. Geol. Mag. 106, 370–384.
Wu, F.Y., Liu, X.C., Ji, W.Q., Wang, J.M., Yang, L., 2017. Highly fractionated granites: recognition and research. Sci. China Earth Sci. 60 (7), 1201–1219.
Xia, Z.L., 2003. Geology of ore deposits of greisen type tin field, Dasongpo, Tengchong. Yunnan Geol. 22, 313–320 (in Chinese with English abstract).
Xie, G.Q., Mao, J.W., Li, R.L., Qü, W.J., Pirajno, F., Du, A.D., 2007. Re-Os molybdenite and Ar-Ar phlogopite dating of Cu-Fe-Au-Mo (W) deposits in southeastern Hubei, China. Mineral. Petrol. 90 (3), 249–270.
Xu, Z.Q., Dilek, Y., Cao, H., Yang, J.S., Robinson, P., Ma, C.Q., Li, H.Q., Jolivet, M., Roger, F., Chen, X.J., 2015a. Paleo-Tethyan evolution of Tibet as recorded in the East Cimmerides and West Cathaysides. J. Asian Earth Sci. 105, 320–337.
Xu, Z.Q., Wang, Q., Cai, Z.H., Dong, H.W., Li, H.Q., Chen, X.J., Duan, X.D., Cao, H., Li, J., Burg, J.P., 2015b. Kinematics of the Tengchong Terrane in SE Tibet from the late Eocene to early Miocene: insights from coeval mid–crustal detachments and

strike–slip shear zones. Tectonophysics 665, 127–148.
Xu, Y.G., Yang, Q.J., Lan, J.B., Luo, Z.Y., Huang, X.L., Shi, Y.R., 2012. Temporal-spatial distribution and tectonic implications of the batholiths in the Gaoligong-Tengliang-Yingjiang area, western Yunnan: constraints from zircon U-Pb ages and Hf isotopes. J. Asian Earth Sci. 53, 151–175.
Yang, J.H., Wu, F.Y., Wilde, S.A., Xie, L.W., Yang, Y.H., Liu, X.M., 2007. Tracing magma mixing in granite genesis: in situ U-Pb dating and Hf-isotope analysis of zircons. Contrib. Mineral. Petrol. 153, 177–190.
Yang, Q.J., Xu, Y.G., Huang, X.L., Luo, Z.Q., Shi, Y.R., 2009. Geochronology and geochemistry of granites in the Tengliang area, western Yunnan: tectonic implication. Acta Petrol. Sin. 25, 1092–1104 (in Chinese with English abstract).
Yin, A., 2006. Cenozoic tectonic evolution of the Himalayan orogen as constrained by along-strike variation of structural geometry, exhumation history, and foreland sedimentation. Earth Sci. Rev. 76, 1–131.
Yin, A., Harrison, T.M., 2000. Geologic evolution of the Himalayan-Tibetan orogen. Annu. Rev. Earth Planet. Sci. 28, 211–280.
Zen, E.A., 1986. Aluminium enrichment in silicate melts by fractional crystallization: some mineralogic and petrographic constraints. J. Petrol. 27 (5), 1095–1117.
Zhang, W.Y., 1996. Metallogenic characteristics and origin of the Tiechang tin deposit in western Yunnan. Geol. Explor. Non-ferrous Metals 5, 335–339 (in Chinese with English abstract).
Zhang, D., Audétat, A., 2017. Chemistry, mineralogy and crystallization conditions of porphyry Mo-forming magmas at Urad-Henderson and Silver Creek, Colorado, USA. J. Petrol. 58 (2), 277–296.
Zhang, Z.M., Ding, L., Zhao, Z.D., Santosh, M., 2017. Tectonic evolution and dynamics of the Tibetan Plateau. Gondwana Res. 41, 1–8.
Zhang, C.L., Li, H.K., Santosh, M., Li, Z.X., Zou, H.B., Wang, H.Y., Ye, H.M., 2012. Precambrian evolution and cratonization of the Tarim Block, NW China: petrology, geochemistry, Nd-isotopes and U-Pb zircon geochronology from Archaean gabbro-TTG-potassic granite suite and Paleoproterozoic metamorphic belt. J. Asian Earth Sci. 47, 5–20.
Zhao, S.W., Lai, S.C., Qin, J.F., Zhu, R.Z., 2014. Zircon U-Pb ages, geochemistry, and Sr–Nd–Pb–Hf isotopic compositions of the Pinghe pluton, Southwest China: implications for the evolution of the early Palaeozoic Proto-Tethys in Southeast Asia. Int. Geol. Rev. 56, 1–20.
Zhao, S.W., Lai, S.C., Qin, J.F., Zhu, R.Z., 2016. Tectonomagmatic evolution of the Gaoligong belt, southeastern margin of the Tibetan plateau: constraints from granitic gneisses and granitoid intrusions. Gondwana Res. 35, 238–256.
Zhao, S.W., Lai, S.C., Qin, J.F., Zhu, R.Z., Wang, J.B., 2017. Geochemical and geochronological characteristics of Late Cretaceous to Early Paleocene granitoids in the Tengchong Block, Southwestern China: implications for crustal anatexis and thickness variations along the eastern Neo-Tethys subduction zone. Tectonophysics 694, 87–100.
Zhao, J.H., Zhou, M.F., 2008. Neoproterozoic adakitic plutons in the northern margin of the Yangtze Block, China: partial melting of a thickened lower crust and implications for secular crustal evolution. Lithos 104, 231–248.
Zhong, D.L., 1998. Paleo-Tethys orogenic Belt in Western Yunnan. Science Press, Beijing, pp. 21–231 (in Chinese).
Zhu, R.Z., Lai, S.C., Qin, J.F., Zhao, S.W., 2015. Early-Cretaceous highly fractionated I-type granites from the northern Tengchong block, western Yunnan, SW China: petrogenesis and tectonic implications. J. Asian Earth Sci. 100, 145–163.
Zhu, R.Z., Lai, S.C., Qin, J.F., Zhao, S.W., 2017a. Petrogenesis of late Paleozoic-to-early Mesozoic granitoids and metagabbroic rocks of the Tengchong Block, SW China: implications for the evolution of the eastern Paleo-Tethys. Int. J. Earth Sci. https://doi.org/10.1007/s00531-017-1501-x.
Zhu, R.Z., Lai, S.C., Santosh, M., Qin, J.F., Zhao, S.W., 2017b. Early Cretaceous Na-rich granitoids and their enclaves in the Tengchong Block, SW China: magmatism in relation to subduction of the Bangong-Nujiang Tethys ocean. Lithos 286–287, 175–190.
Zhu, D.C., Mo, X.X., Wang, L., Zhao, Z., Niu, Y., Zhou, C., Yang, Y., 2009. Petrogenesis of highly fractionated I-type granites in the Zayu area of eastern Gangdese, Tibet: constraints from zircon U-Pb geochronology, geochemistry and Sr-Nd-Hf isotopes. Sci. China Ser. D-Earth Sci. 52, 1223–1239.
Zhu, F.L., Tao, Y., Hu, R.Z., Liao, M.Y., 2011. Formation age of the Luziyuan lead-zinc deposit in Zhengkang, Yunnan. Bull. Miner. Petrol. Geochem. 30, 73–79 (in Chinese with English abstract).
Zou, H., Fang, Y., Zhang, S.T., Zhang, Q., 2017. The source of Fengjia and Langxi barite–fluorite deposits in southeastern Sichuan, China: evidence from rare earth elements and S, Sr, and Sm–Nd isotopic data. Geol. J. 52 (3), 470–488.